Document downloaded from:

http://hdl.handle.net/10251/99123

This paper must be cited as:

Díaz Morales, UM.; Corma Canós, A. (2016). Ordered covalent organic frameworks, COFs and PAFs. From preparation to application. Coordination Chemistry Reviews. 311:85-124. doi:10.1016/j.ccr.2015.12.010

The final publication is available at

https://doi.org/10.1016/j.ccr.2015.12.010

Copyright Elsevier

Additional Information

Ordered covalent organic frameworks, COFs and PAFs. From preparations to applications.

Urbano Díaz [*], *Avelino Corma* [*]

Instituto de Tecnología Química, UPV-CSIC, Universidad Politécnica de Valencia, Avenida de los Naranjos s/n, E-46022 Valencia, Spain

Corresponding author. Tel.: +34963877800; fax: +34963877809.
E-mail addresses: acorma@itq.upv.es (A. Corma); udiaz@itq.upv.es (U. Díaz).

Contents

Abstract

In the last years, covalent organic frameworks, COFs, and their derived sub-groups based on auto-assembly of exclusively aromatic units, PAFs, are emerging into the advanced materials field due to their high free porous volume, structural regularity, robustness, hydrothermal stability, and functional variety. Their high gas uptake capacities, presence of stabilized active functions in the framework and charged low-density structures combined with their organization through π-conjugated system arrays open the possibilities of COFs and PAFs to be used as effective materials for adsorption, selective separation and catalysis, and in nanotechnological applications. This review will be focused on self-assembly synthesis mechanisms, physico-chemical characteristics, and applications of this class of promising covalent porous organic structures, outlooking their possible future approaches and perspectives.

Keywords: Covalent Organic Frameworks, Porous Aromatic Frameworks, Adsorption, Gas uptake, Catalysis, Nanotechnology.

1. Introduction

The generation of stable, robust, ordered and highly accessible porous materials with associated functionalities in their framework remains a crucial topic in material science when searching advanced solids for adsorption, separation, catalysis, energy storage, sensors, electronic or photoluminescence devices [1,2]. In all cases, homogeneous porous distribution and functional networks are indispensable requirements to establish suitable and efficient host-guest interactions and confinement effects [3]. For the preparation of this type of ordered porous materials, the use of suitable building blocks is fundamental to construct various networks through convenient synthesis methodologies [4,5].

Specific organic, inorganic or, even, organic-inorganic building blocks, such as macromolecules, modified metallic nanoparticles or bridged silsesquioxanes, respectively, have been used to obtain several families of stable porous materials with associated functionalities [6,7]. Remarkably, the effective covalent combination of organic bridges and tetrahedral silicon units allowed the preparation of organozeolites (OZs) and multi-functional periodic mesoporous organosilicas (PMOs), following sol-gel, hydrolysis and poly-condensation, micellar or hydrothermal synthesis processes [8,9]. However, the difficulty to homogenously distribute into the walls the different organic and inorganic counterparts is still an important issue to avoid undesired formation of specific structural domains where one class of functions predominates and negatively affects the global properties of the hybrid solids [10]. On the other hand, metalorganic frameworks (MOFs) and coordination polymers were also formed through the effective combination of organic linkers and metallic nodes by, most frequently, solvothermal synthesis processes to form very accessible multi-functional hybrid materials [11]. The number of metalorganic structures generated rises quickly due to the ease of combining metallic clusters with organic bi-dentate ligands. Nevertheless, low density and flexibility exhibited by the MOFs strongly favor the formation of unstable frameworks, which can easily be altered [12].

Recently, another family of highly accessible porous materials, based on the effective assembly of different specific builders, has emerged. These solids are formed by the covalent combination of rigid and stable organic builders to construct novel robust porous covalent organic frameworks (COFs) [13]. In this case, the use of building units with enough rigidity and covalent assembly capacity has allowed the generation of homogenous and highly accessible porous ordered materials whose organic structural components are able to support several type of functionalities. Moreover, the preparation of novel COF-type materials based on rich-electronic conjugated backbones could imply the development of stable solids with

optoelectronic and photochemical applications. Within this important group of organic materials, those based on exclusively aromatic builder units, named as porous aromatic frameworks (PAFs), are especially remarkable and are still more robust and stable than conventional COFs or even MOFs, maintaining intrinsic electron rich structure, capability to be functionalized and high porosity [14]. Although PAFs materials exhibit irregular internal structure compared with highly ordered crystalline COFs (this latter topologically more similar to MOFs), their purely organic composition, comparable physico-chemical properties and analogous potential uses in nanotechnology, gases uptake, and catalytic applications, justify the combined analysis of this emergent group of COFs and PAFs families.

2. Covalent Organic Frameworks: COFs

2.1. COFs: Synthesis, structure and properties

2.1.1. Three-Dimensional COFs

Organic polymers with intrinsic microporosity, based on associated rigid spyrocyclic, arylene or, in general, aromatic linkers by self-condensation processes, have been described in the last years. However, their frameworks exhibited low crystallinities and poor porous homogeneity, similar to conjugated microporous or hyperbranched polymers [15,16,17]. These drawbacks were overcome when organic builders were covalently assembled to generate ordered networks through solvothermal condensation reactions. For example, when phenyl diboronic acid, $[C_6H_4[B(OH)_2]_2]$, and hexahydroxytriphenylene, $[C_{18}H_6(OH)_6]$, monomers were condensed, the first covalent organic framework (COF) resulted [18]. Specifically, highly crystalline solids constructed by swelled porous graphite-type layers with staggered (COF-1, *$P6_3/mmc$*) or eclipsed (COF-5, *P6/mmm*) conformations were obtained, being their frameworks based on strong bonds between boron, carbon and oxygen atoms to generate rigid porous solids with pore sizes from 7 to 27 Å. COF-1 and COF-5 exhibited high hydrothermal stability, stable and regular porosity, with surface areas between 700 and 1600 m^2g^{-1} (Fig. 1), being a promising alternative to MOF materials with similar specific surface areas but improved robustness. Comparative studies to correctly measure the pore size distribution were carried out with COF-1-type solids (average pore size between 1.0 and 2.0 nm), being confirmed that a Density Functional Theory (DFT) model was more appropriate than Horvath-Kawazoe (HK) and Barret-Joyner-Halenda (BJH) models due to the limitation of porosity range present in the porous organic frameworks [19]. Additionally, more efficient COF-1 synthesis routes at room temperature mediated N-Lewis bases (NH_4OH) were carried out, being observed the formation of smaller COF-1 particles although the crystallinity and textural properties were preserved [20].

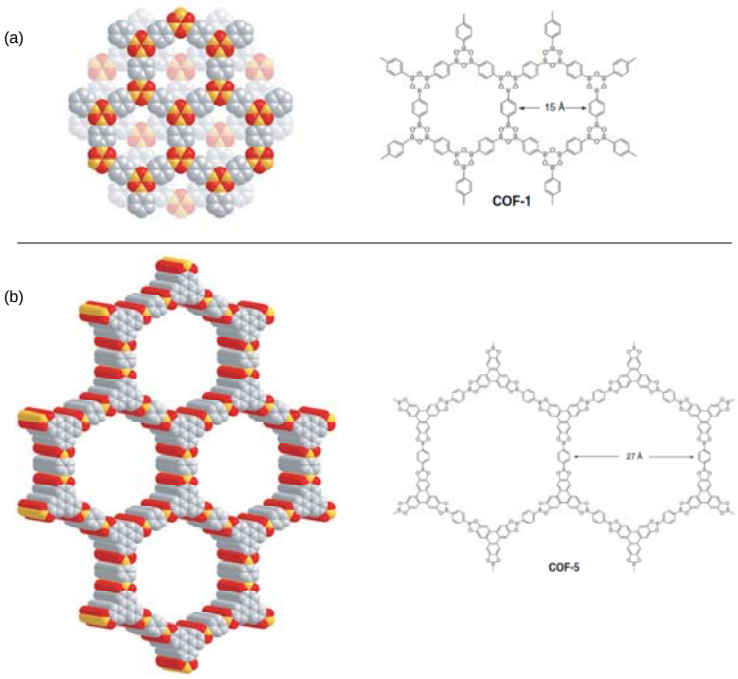

Figure 1. Images of (a) COF-1 and (b) COF-5 along *c* axes. Carbon, boron, and oxygen are shown as gray, orange, and red colors, respectively. Reproduced from [18] with permission from Science.

Following this solvothermal synthesis methodology, self-assembly of tetrahedral tetra(4-dihydroxyborylphenyl)methane or tetra(4-dihydroxyborylphenyl)silane and by condensation of triangular 2,3,6,7,10,11-hexahydroxytriphenylene, favored the formation of novel three-dimensional COFs (COF-102, -103, -105 and -108) by targeting two framework types (*ctn* and *bor*) based on triangular and tetrahedral nodes which acted as building units (Fig. 2). Although these materials exhibited very low densities (0.17 g/cm^3 for COF-108), they showed high thermal stabilities and high porosity due to the robust network formed by covalent bindings (C-C, C-O, C-B, and B-O). Interestingly, the experiments carried out during the synthesis process of these 3D COFs revealed that both thermodynamic and kinetic factors are decisive to achieve the crystallization of the materials, being necessary a suitable correspondence among these two parameters [21]. For COF-102 material, an accurate molecular mechanics force field was applied to predict, without experimental data, its network topology. The results showed that the *ctn* structure was preferred thermodynamically by 11.2 kcal mol^{-1} over the *bor* topology due to a lower steric strain [22]. Interestingly, computational studies about the thermal expansion behavior of different covalent organic frameworks demonstrated that COF-102 showed negative thermal expansion (NTE), the motion of the aromatic carbon rings with the temperature being responsible for this behavior that can also

be valid in other 3D COFs. This peculiar characteristic confirms that COF materials are a kind of contracting materials which are similar in thermal expansion effects to conventional 3D MOFs and other coordination polymeric frameworks (Fig. 3) [23].

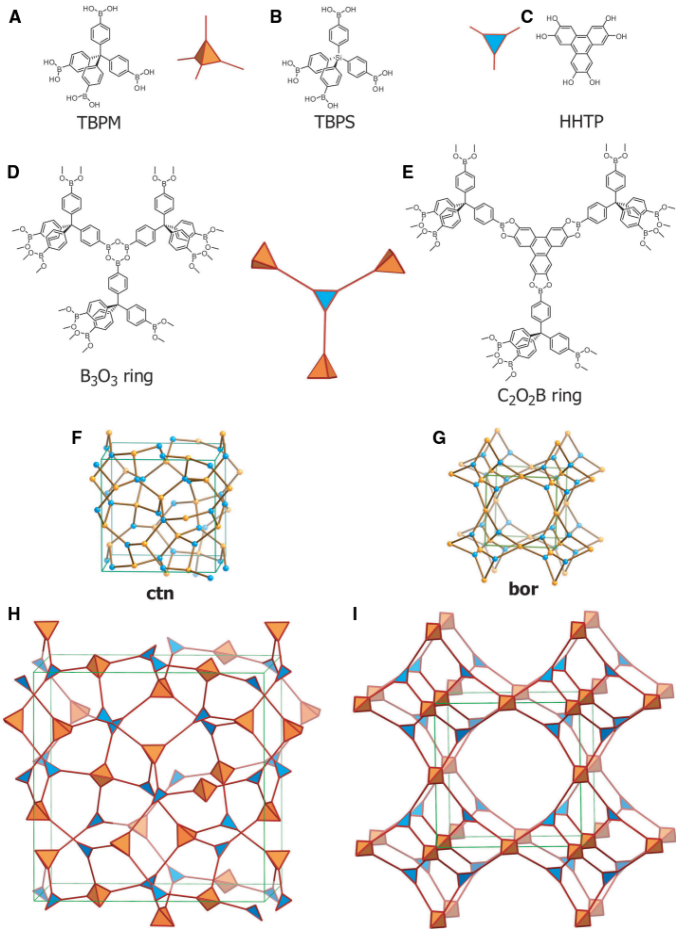

Figure 2. Condensation pathways obtaining 3D COFs. Boronic acids are indicated in orange as tetrahedral units, (A) and (B), and a planar triangular unit (C) is indicated in blue. Fragments showing B_3O_3 (D) and C_2O_2B (E) connections are also represented. The structural units can be located on the *ctn* (F) and *bor* (G) frameworks, as it is shown in the respective swelled networks (H) and (I), respectively. Reproduced from [21] with permission from Science.

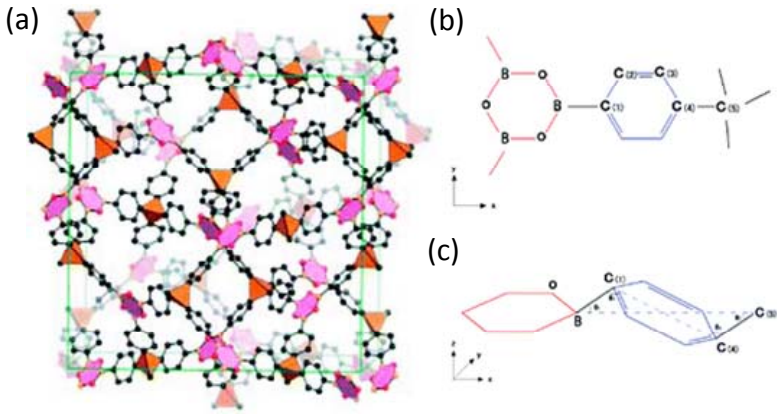

Figure 3. (a) Structural representation of COF-102. Carbon, boron, and oxygen atoms are shown in gray, orange, and red colors, respectively. (b) Partial model system of COF-102. (c) The thermal motion of aromatic carbon ring linkers (red ring: B_3O_3 ring (in the *xy* plane); blue ring: aromatic carbon ring). Reproduced from [23] with permission from ACS.

Advancing in the COFs' synthesis, novel COF structures have been synthesized with carbon nitride topology from condensation of divergent boronic acid, tetra(4-dihydroxyborylphenyl)methane, and tert-butylsilane triol, $tBuSi(OH)_3$, to generate a new crystalline COF-202, $[C(C_6H_4)_4]_3[B_3O_6\ (tBuSi)_2]_4$. This solid was constructed through strong covalent bonds Si-O and B-O that linked triangular and tetrahedral building units, favoring structures which showed high stability, low molecular density and high porosity with specific surface areas around of 2700 $m^2\ g^{-1}$ (Fig. 4) [24].

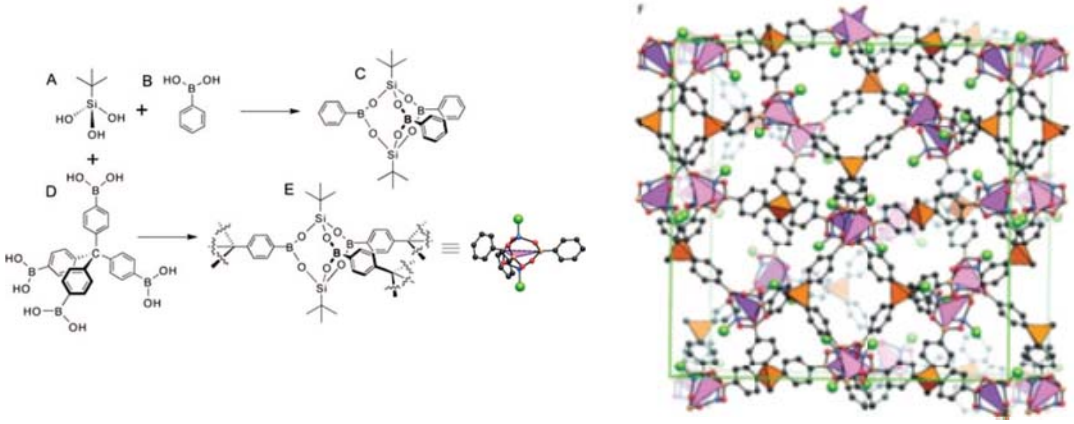

Figure 4. Synthesis route based on the self-assembly of *tert*-butylsilane triol **A** with monotopic boronic acid **B** to form the borosilicate-type cage **C**. Assembly of **A** with boronic acid **D** generates the unit **E** with boron atoms occupying the vertices of a triangle and linked together with the tetrahedral units **D** to form the COF-202 **F**. C, black; Si, blue; O, red; B, yellow; *tert*-butyl groups are shown in green. Reproduced from [24] with permission from ACS.

The incorporation of Lewis acid catalysts, during the solvothermal condensation synthesis route to form COFs materials, implies the formation of novel organic structures

through different formation mechanisms. Following this alternative approach, COF-5 and COF-10 materials were obtained using a new method that employs poly-functional boronic acid and acetonide-protected catechol reactants in presence of Lewis acid catalyst such as $BF_3{\cdot}OEt_2$ to form ordered materials based on three boronate ester-linked covalent organic frameworks. This transformation avoided also the use of unstable and insoluble poly-functional catechols. Interesting mechanistic study of this synthesis process showed that the dehydrated trimerization of boronic acids to boroxines and the formation of a non-productive aryl boronic acid-BF_3 complex strongly affected the rate of boronate ester formation. Moreover, crossover additional synthesis, employing substituted boronate ester derivates, suggests that ester hydrolysis was the most likely exchange mechanism during COF formation under $BF_3{\cdot}OEt_2$-catalyzed conditions (Fig. 5) [25]. Also, through borate ester formation synthesis route, novel azo-benzene COFs were synthesized by *trans*-to-*cis* photoisomerization of azo monomers under irradiation with 365 nm UV light, being observed that this process decreased the crystallinity of azo-COF materials but without changing their pore size [26].

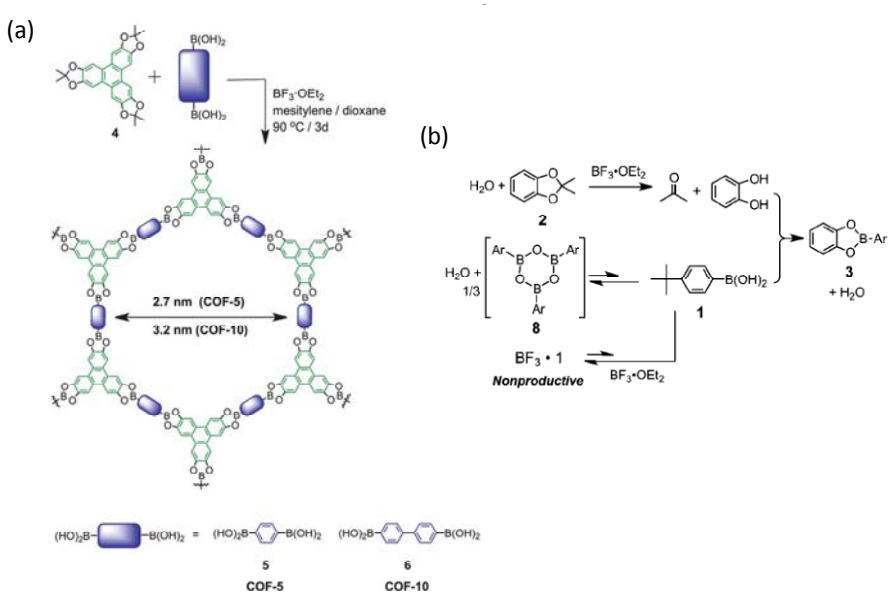

Figure 5. (a) Synthesis of COF-5 and COF-10 under $BF_3{\cdot}OEt_2$-catalyzed conditions. (b) Proposed mechanism of $BF_3{\cdot}OEt_2$ catalyzed boronate ester formation. Reproduced from [25] with permission from RSC.

Imine linkages were also present to form crystalline 3D porous covalent organic frameworks without the use of boronic acid derivatives. It was the case of COF-300, synthesized through the condensation of tetrahedral tetra-(4-anilyl)-methane and linear terephthaldehyde builder units, whose structure was formed by five independent diamond frameworks. Despite the detected interpenetration, the framework contained permanent pores of 7.2 Å and surface area of approximately 1360 $m^2\ g^{-1}$ (Fig. 6) [27]. Imine condensation

was also followed to obtain a novel so-called COF-320 through solvothermal condensation of tetra-(4-anilyl)-methane and 4,4'-biphenyldialdehyde in 1,4-dioxane at 120 °C to form a 9-fold interlaced diamond network, the final crystalline material exhibiting high porosity with a Langmuir surface area of 2400 m^2g-1. The crystal structure of COF-320 solid was elucidated by single-crystal 3D electron diffraction (Fig. 7) [28]. On the other hand, azine-linked covalent frameworks were also obtained in absence of boronic derived precursors from direct assembly of hydrazine with 1,3,6,8-tetrakis-(4-formylphenyl)-pyrene. In this case, pyrene fragments were located in the vertices and the diazabutadiene (-C=N-N=C-) units in the edges of rhombic polygonal layers, like in an AA-stacking mode to form regular ordered pyrene columns combined with 1D microporous channels (Fig. 8) [29].

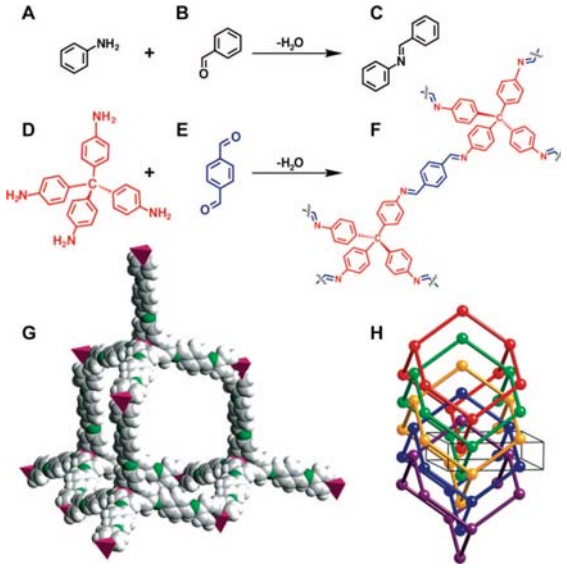

Figure 6. Assembly of aniline **A** with benzaldehyde **B** generating *N*-benzylidene-aniline **C**. Condensation of **D** with ditopic **E** produces the rod-type bis-imines **F** which will be linked with tetrahedral units to form the diamond network of COF-300. **G** is the structural representation of COF-300 (C gray and pink, N green, H white) and **H** is the image of the 5-fold interpenetrated diamond framwork. Reproduced from [27] with permission from ACS.

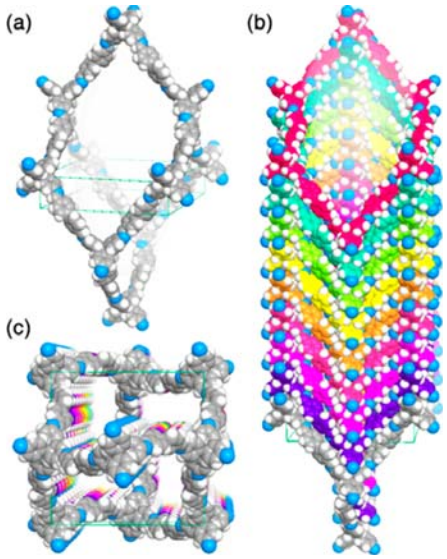

Figure 7. Crystalline representation of COF-320 obtained from rotation electron diffraction (RED). (a) Adamantane cage in the diamond network. (b) COF-320 along the *a*-axis showing a 9-fold interpenetration. (c) 1D rectangle-type channels along the *c*-axis. Reproduced from [28] with permission from ACS.

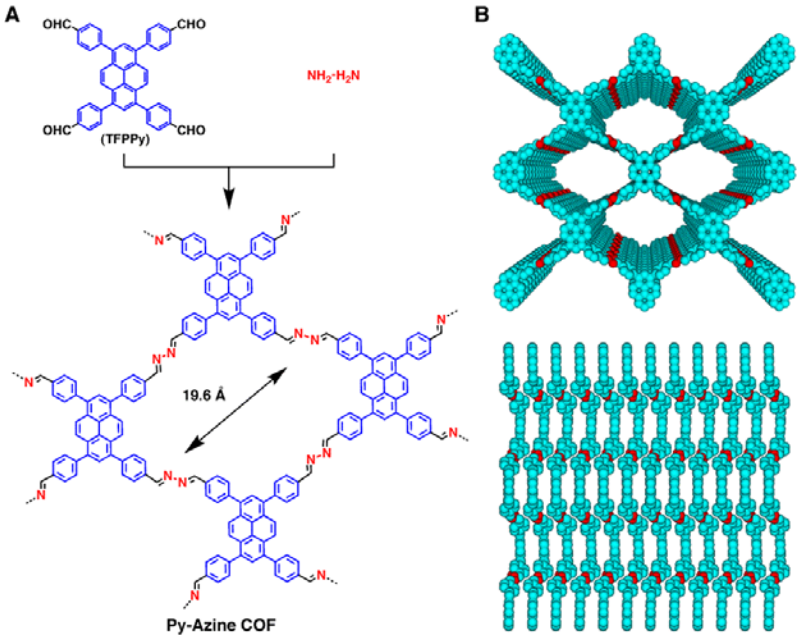

Figure 8. (a) Synthesis pathway of the azine-linked COF (pyrene-azine COF); (b) Top and side views of the AA stacking structure of the pyrene-azine COF. Reproduced from [29] with permission from ACS.

The textural properties exhibited by the COFs' materials above described show the formation of organic open pore structures associated to covalent bonding frameworks, exhibiting pore sizes up to 3.4 nm. With the objective to increase the accessibility of this type of materials towards mesoporous range, Bein's group synthesized for the first time a new ordered mesoporous BTP-COF with free pore diameters of 4.0 nm. This material was obtained

under solvothermal processes by self-assembly of 1,3,5-benzenetris(4-phenylboronic acid) (BTPA) and the polyol 2,3,6,7-tetrahydroxy-9,10-dimethyl-anthracene (THDMA) (Fig. 9) [30].

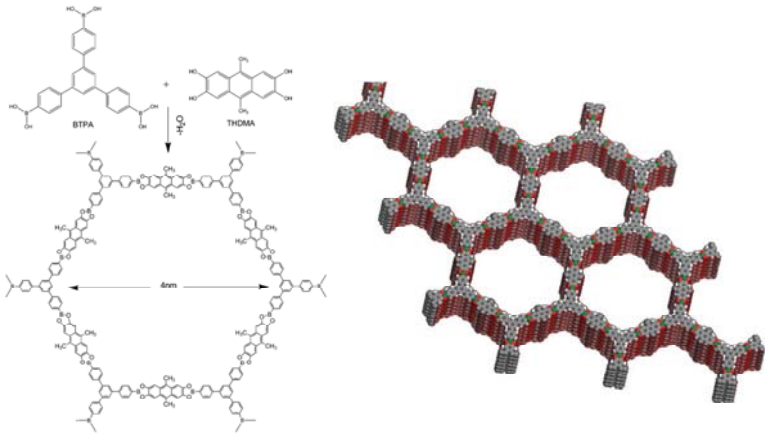

Figure 9. Solvothermal synthesis scheme of BTP-COF and structural representation. Reproduced from [30] with permission from RSC.

2.1.2. Two-Dimensional COFs

The capacity of rigid organic units to condense as individual nanosheets allows generating stable COF-type 2D covalent organic structures formed by ordered piled layers, opening the possibilities of COF materials due to the associated versatility of two-dimensional solids. Following this research line, Smith *et al.* established that it is possible the formation of 2D COF frameworks by the control of nucleation and crystallization steps under optimal solvothermal synthesis conditions, such as occurred with COF-5 [31]. In general, these families of lamellar COFs can be post-modified through swelling, pillarization, exfoliation or delamination processes to increase the porosity and/or functionality of the organic materials based on single nanosheets.

In 2007, Cote *et al*. synthesized three novel crystalline micro and mesoporous 2-dimensional COFs, so-called COF-6, -8, and -10, from boronic acid derivatives and 2,3,6,7,10,11-hexahydroxytriphenylene (HHTP) as building block precursors (Fig. 10). These 2D COFs' materials were based on C_2O_2B rings, forming eclipsed layered structures with pore sizes ranging from 6.4 to 34.1 Å. These exhibited high thermal stability, low densities and high porosity with specific surface areas of 980, 1400, and 2100 $m^2\ g^{-1}$ for COF-6, -8, and -10, respectively [32]. Furthermore, this type of 2-dimensional layered covalent organic frameworks organized by π-electron systems into ordered frameworks have allowed the preparation of the larger pores in COF-type structures. For instance, it is the case of the 2D mesoporous material obtained by the assembly of HHTP and 4,4'-diphenylbutadiynebis(boronic acid) (DPB) that exhibited regular pore size distribution centered

at 4.7 nm (Fig. 11). Complementary molecular dynamics and density functional theory calculations provided insight into the interlayer spacing of the COF and suggested that adjacent layers were horizontally offset by 1.7-1.8 Å, in contrast to the eclipsed AA-stacking typically proposed for these materials [33], as it occurs in the 2D porous borazine-linked COFs [34].

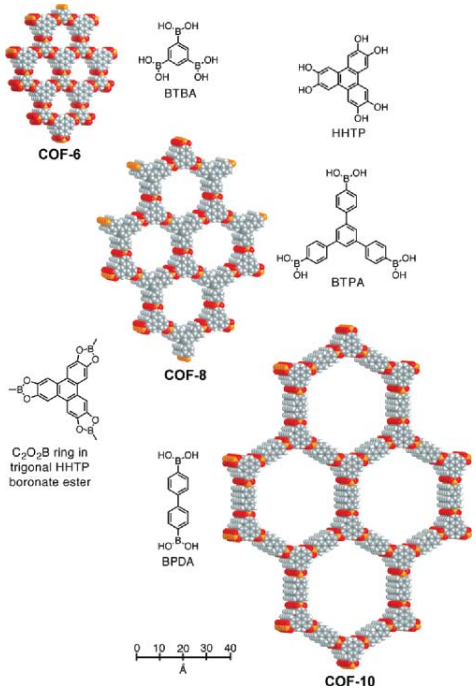

Figure 10. Self-assembly of boronic acid units (BTBA, BTPA, BPDA) with HHTP to form 2D COFs (COF-6, -8, and -10). C, gray; H, white; B, orange; O, red. Reproduced from [32] with permission from ACS.

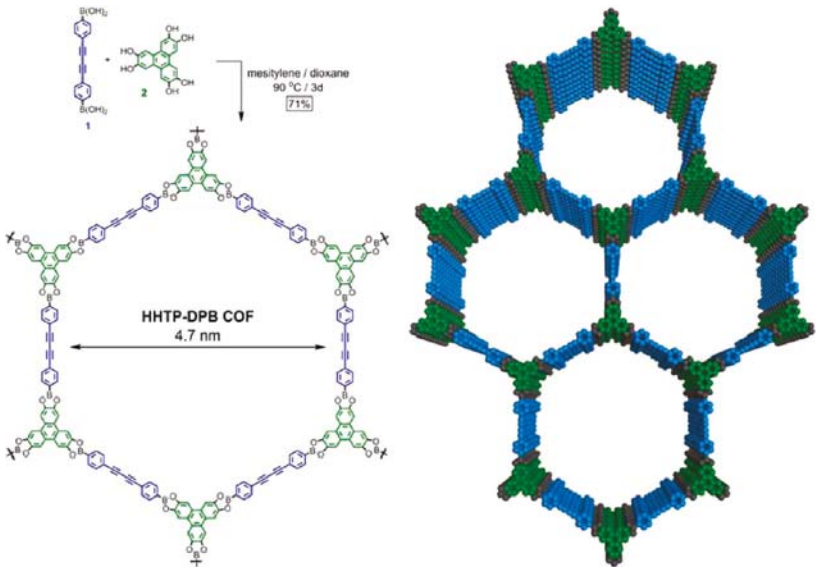

Figure 11. Synthesis of HHTP-DPB COF from bis(boronic acid) linker and HHTP (left) and model of the idealized *bnn* topology (right). Reproduced from [33] with permission from ACS.

Although 2D COFs constructed by B–O bond formation have been highly studied, their weak chemical stability leads to rapid decomposition upon exposure to water vapor and limits their effective usage in gas uptake, catalysis or other applications. To overcome this limitation, and improving framework robustness, 2-dimensional COFs based on C-N bonds have been prepared. Thus, novel azine-linked COF, so-called ACOF-1, was obtained by assembly of hydrazine and 1,3,5-triformylbenzene following solvothermal synthesis processes (Fig. 12) [35]. Hydrazone linkages were also useful to form extended two-dimensional stable porous frameworks through solvothermal condensation routes between 2,5-diethoxyterephthalohydrazide with 1,3,5-triformylbenzene or 1,3,5-tris(4-formylphenyl)benzene, generating two novel covalent solids, COF-42 and -43, that avoid the most conventional boronate ester structural network. Since the hydrazine moiety is approximately coplanar with the aromatic rings, due to resonance effects and internal hydrogen bonding, the formation of 2D trigonal layers was favored. These layers can pack in eclipsed *bnn* (P6/m) or staggered *gra* ($P6_3/m$) modes (Fig. 13) [36], similarly to 2-dimensional mesoporous networks based on triptycene derivated building units [37]. Interestingly, these two topologies were also described for two-dimensional mesoporous imine-linked COFs (ILCOF-1) obtained through the condensation reaction between 1,3,6,8-tetrakis(*p*-formylphenyl)pyrene and *p*-phenylenediamine in 1,4-dioxane in presence of aqueous acetic acid at 120°C. The thermal stability of ILCOF-1 was confirmed by thermogravimetric analyses, showing that this COF remained stable at temperatures of up to approximately 400°C under air. The crystalline nature of the ILCOF-1 was evidenced by SEM micrographs, being observed the formation of aggregated cubes of about 30-70 nm in size (Fig. 14) [38].

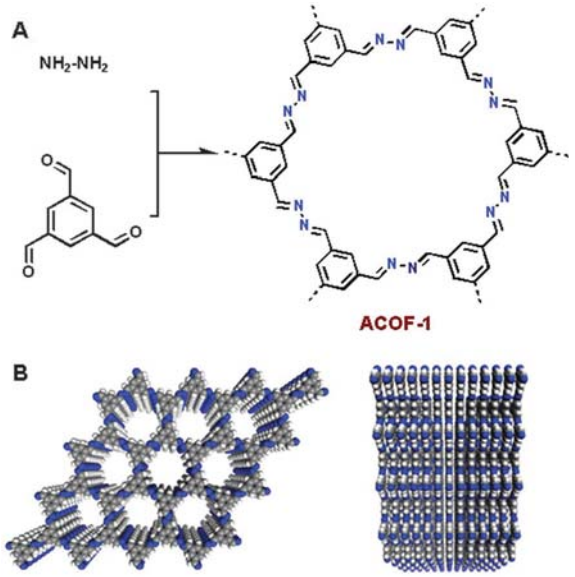

Figure 12. (a) Synthesis route of ACOF-1. (b) Top and side views of the AA stacking structure of ACOF-1. Reproduced from [35] with permission from RSC.

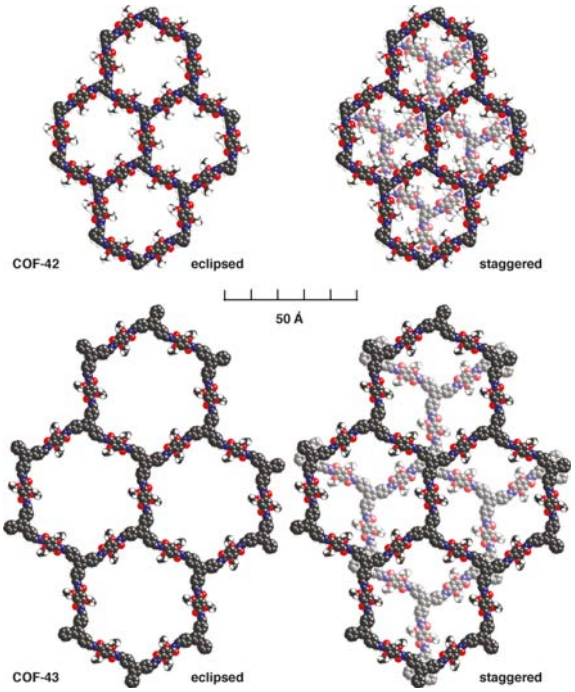

Figure 13. Representation of space-filling models of COF-42 and COF-43 in both extreme packing modes, eclipsed (*bnn* topology) and staggered (*gra* topology). Atom colors: C, black; H, white; O, red; N, blue. Reproduced from [36] with permission from ACS.

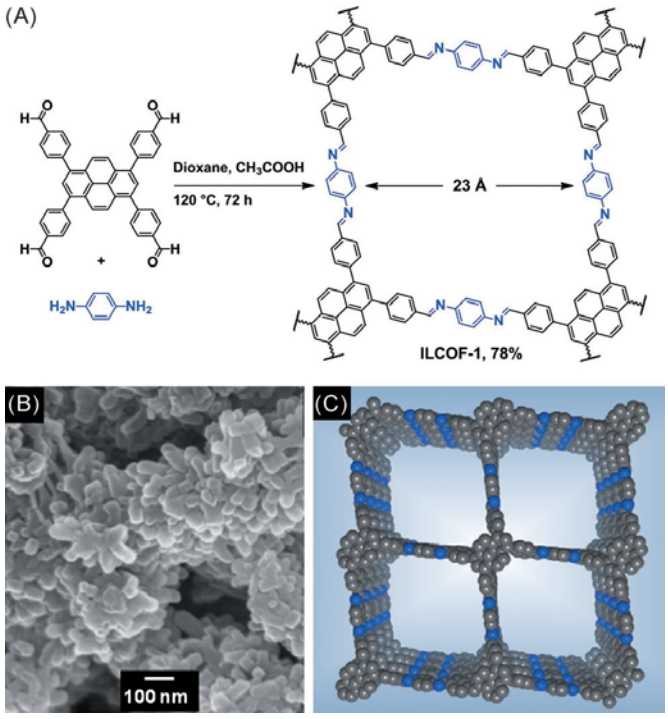

Figure 14. (a) Synthesis of ILCOF-1; (b) SEM micrograph of as-prepared materials, and (c) space filing representation of the resulting 2D network; C, gray; N, blue. Reproduced from [38] with permission from Wiley.

Among the family of lamellar COFs, porphyrin-based two-dimensional covalent organic frameworks are an important and numerous group due to the rigidity, stability and assembly's ability of porphyrin macrocycle-type units to form layers, taking part during solvothermolytic synthesis routes. The inclusion of 18-electron π-systems in the COFs' framework could open the possibilities of these organic porous materials as semiconductors or emission solids. It is the case of the 2D COF obtained from Zinc (II) 5,10,15,20-tetrakis(4-(dihydroxyboryl)phenyl) porphyrin (TDHB-ZnP) together with 1,2,4,5-tetrahydroxybenzene (THB) as building units (Fig. 15) [39]. Following similar approaches, insoluble 2D Zn-phthalocyanine (ZnPc) covalent organic framework powders with expanded diagonal pore widths of 2.7, 3.4, 4.0, and 4.4 nm were prepared by using longer linkers incorporated into COFs structures, being possible tuning the porosity and composition of these materials in function of the used linkers (Fig. 16) [40]. Similarly, co-condensation processes of Ni-phthalocyanies with electron-deficient benzothiadiazole (BTDA) blocks led to formation of 2D structures based on AA-stacking of polymer sheets [41]. Following this type of 2-dimensional COFs, interesting layered Cu-porphyrin arrays were also located taking part of the COFs' networks using squaraine fragments as stable linkers. Moreover, this lamellar Cu-COFs were highly stable, retaining their crystallinity in common organic solvents, such as methanol, benzene, and hexane, independently of their polarity, and even in water and aqueous HCl solution (1 M). In contrast, more conventional 3D boronate- and boroxine-linked COFs, which did not have a π-conjugated skeleton, did not keep the crystalline structure upon exposure to water, alcohol, or acid media [42]. On the other hand, crystalline and robust 2D COFs were also obtained through solvothermal condensation between Co-phthalocyanine and porphyrin diboronic acid monomers [43, 44].

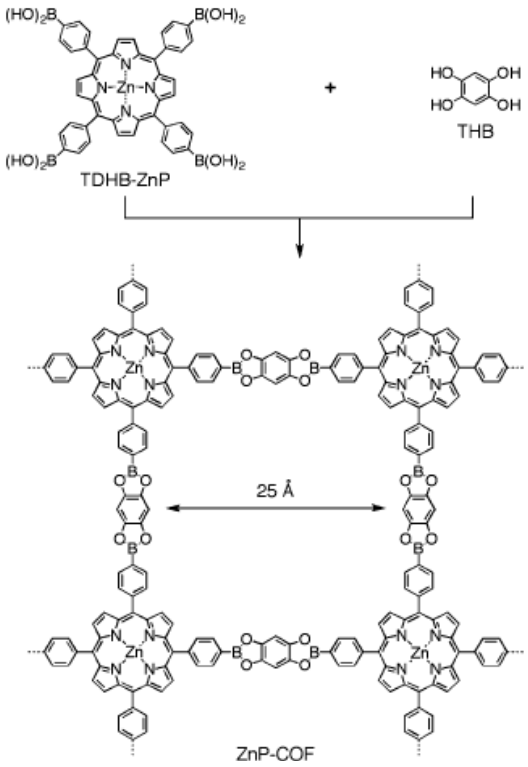

Figure 15. Synthesis pathway of a porphyrin-based on 2D COF (ZnP-COF). Reproduced from [39] with permission from RSC.

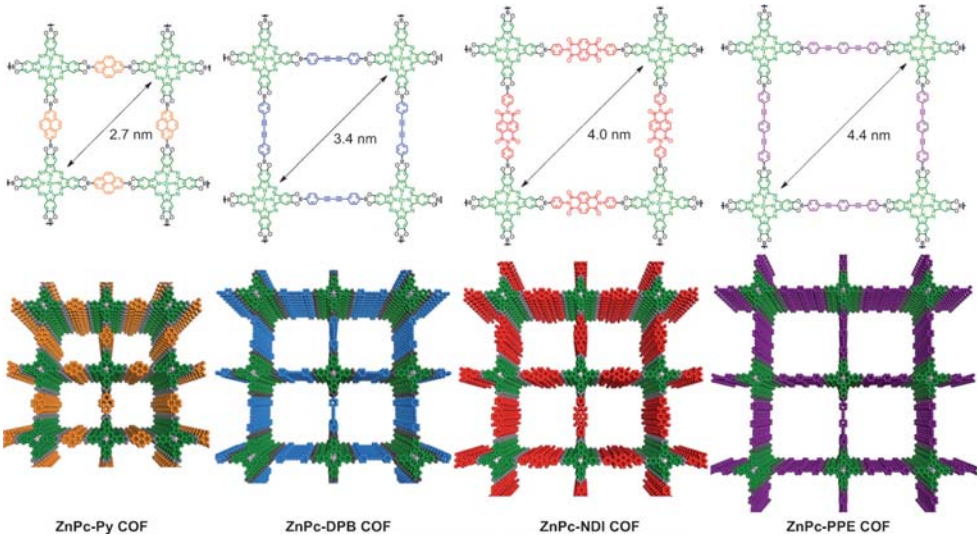

Figure 16. Chemical and extended structures of the expanded ZnPc COFs. Each COF forms a two-dimensional layered network containing zinc phthalocyanines connected by (left to right) pyrene, diphenylbutadiyne, naphthalenediimide, and phenylbis(phenylethynyl) units. Reproduced from [40] with permission from Wiley.

It is remarkable that, through 2D COFs synthesis routes, it has been possible to obtain hierarchical micro and mesoporous organic frameworks in a direct one-step process, opening the possibilities to regulate *a priori* the textural properties of COFs materials. In this sense, a

novel COF with two different kinds of ordered pores with controllable sizes was described based on one porous system with triangle shape within microporous range (7.1 Å) and the other in mesoporous range (26.9 Å) with hexagonal conformation (Fig. 17) [45].

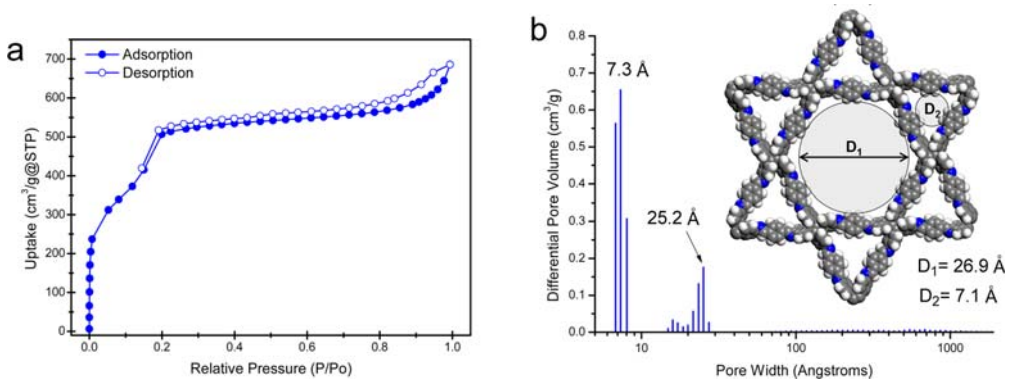

Figure 17. (a) N_2 adsorption-desorption isotherms and (b) pore size distribution of the dual-pore COFs. Reproduced from [45] with permission from ACS.

The expanded lamellar materials, generating individual 2D monolayers of associated polymers, have been practically unexplored. However, Bunck *et al*. were able to generate few- and/or single-layer 2-dimensional polymers from COF-43 layered precursor by immersion of the initial powder in different solvents. Specifically, it was observed that samples exposed to THF, $CHCl_3$, PhMe and MeOH retained their original diffraction patterns, while those exposed to dioxane, H_2O, and DMF appeared amorphous. Although crystallinity loss might arise from framework hydrolysis, the high stability of hydrazine backbone of COF-43-type materials allowed maintaining the internal covalent linkages without interrupting each individual monolayers, which preserved their characteristic periodic hexagonal structure. This methodology is useful to obtain individual and isolated COF nanosheets (Fig. 18) [46].

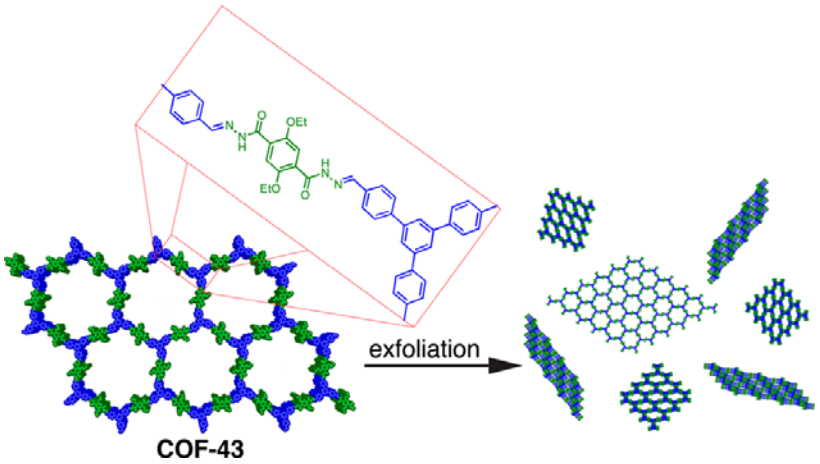

Figure 18. Delamination scheme of COF-43 generating suspension formed by 2D layers. Reproduced from [46] with permission from ACS.

In Table 1, specific surface area and pore size distribution of relevant above described COFs are summarized to better know their textural properties and establish a suitable comparison between them. In general, microporous 3D COFs exhibit higher surface areas and lower pore sizes than 2D COFs.

Table 1
Textural properties of relevant COF materials.

Dimensionality	COF-type	BET Surface Area (m^2g^{-1})	Pore Size (Å)	Ref.
3D	COF-1	700	6-15	[18]
	COF-5	1600	27	
	COF-102	3500	12	[21]
	COF-103	4200		
	COF-202	2700	11	[24]
	COF-300	1400	7	[27]
	COF-320	2400[a]	11	[28]
	BTP-COF	2000	40	[30]
2D	COF-6	1000	9	[32]
	COF-8	1400	16	
	COF-10	2100	32	
	COF-42	700	23	[36]
	COF-43	600	38	
	ILCOF-1	2700	23	[38]
	Porphyrin COFs	400-500	27-44	[40]

[a]Langmuir Surface Area

2.1.3. Thin films and nanofibers based on COFs

Different direct approaches have been followed to fabricate 2D long-range-ordered COFs thin films or even single monolayers by surface mediated synthesis [47]. It is the case of 2-dimensional covalent organic frameworks obtained from halogenated aromatic monomers synthesized on graphite (001), Cu (111) or Ag (110) under ultra-high vacuum conditions (Fig. 19) [48]. In addition, two-dimensional polymers obtained by dehydration of 1,4-benzenediboronic acid (BDBA) by vapor deposition on well-oriented noble metal surfaces allowed the conclusion that Ag (111) and Ag (100) surfaces are better templates than Au (111) surfaces for 2D COFs thin films formation, and far more than Cu (111) surfaces, probably due to the metal nature and surface diffusion of adsorbed organic precursors [49,50]. The surface growth of the 2D thin film COFs was established as a sequential polymerization in two stages. This conclusion was achieved using *p*-bromo-benzene boronic acid (BBBA) as bi-functional precursor that was vapor deposited on Au(111) surface. Initially, boronic acid reacted to generate trimers connected by covalent boroxine units. After, an Ullmann coupling process was thermally activated to favor the formation of C-C bonds among the trimers, obtaining the final polymeric 2D COF structure. In this case, a well-extended network was obtained, differing

from the ideal honeycomb-like network by a substantial number of non-hexagonal pores, which were intrinsic defects to the polymer structure (Fig. 20) [51].

Recently, in this area, Bein *et al.* used an innovative facile method to prepare some 2D COFs as films by vapor-assisted method at room temperature. Specifically, homogeneous films of benzodithiophene (BDT)-COF and COF-5 with tunable thickness were prepared on glass substrates. BDT-COF films exhibited high porosity, while in contrast thinner BDT-COF films appeared as dense layers. So, room temperature vapor assisted conversion is a suitable way to generate several 2D COF films with different morphology [52]. On the other hand, interesting 2-dimensional COF nanofibers were prepared by solvothermal approach through morphological transformation from microspheres to nanofibers supported by dissolution-recrystallization mechanisms due to the reversible nature of dynamic imine bonding. COF nanofibers can suffer epitaxial grow on the aramid microfiber surface. (Fig. 21) [53].

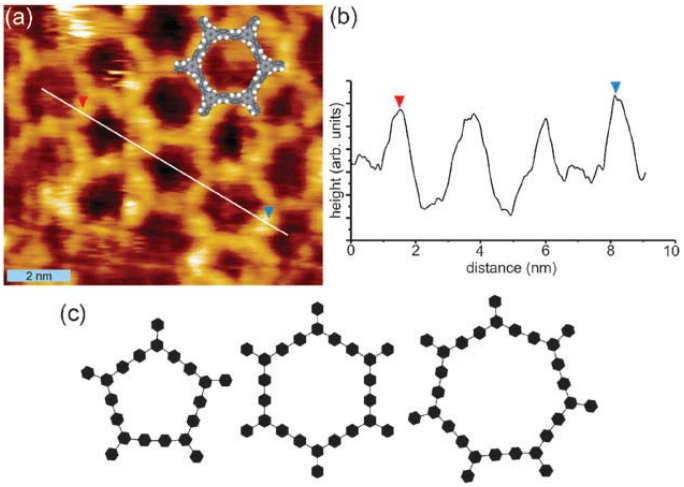

Figure 19. (a) STM topograph of 1,3,5-tris(4-bromophenyl)benzene (TBB) COF on Cu(111) after evaporation and consecutive annealing. (b) Linescan showed in (a) across three rings with a center-to-center distance of 2.2 nm for one single ring. (c) Main structural units: pentagon, hexagon and heptagon. Reproduced from [48] with permission from RSC.

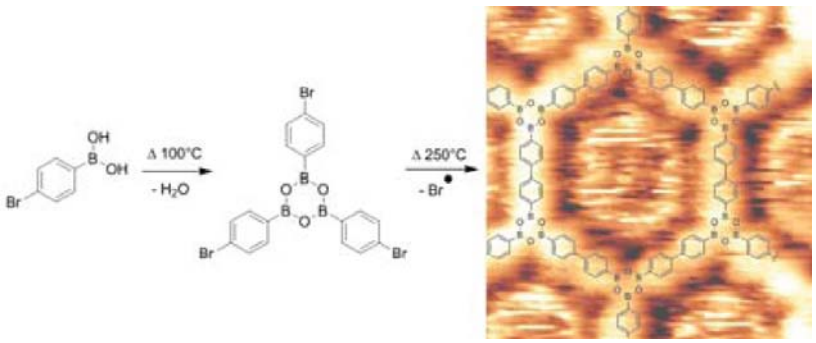

Figure 20. Surface COF formed by a consecutive polymerization process in two stages. Reproduced from [51] with permission from ACS.

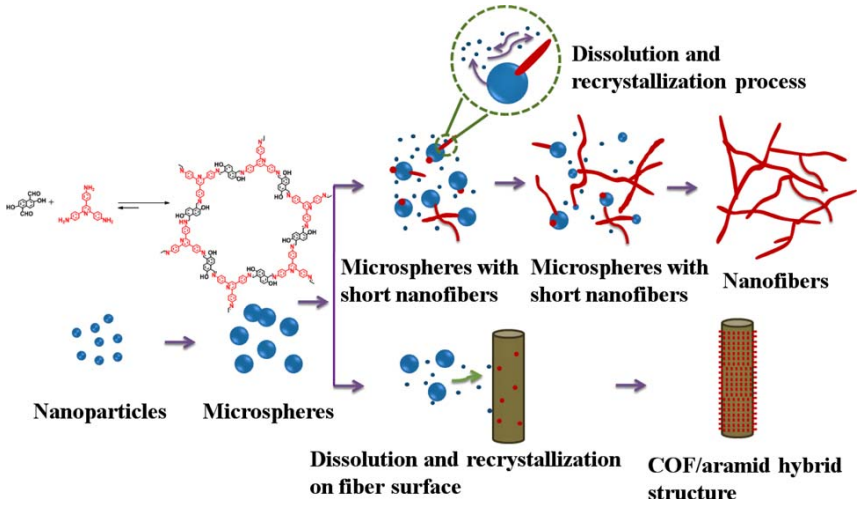

Figure 21. Formation of COF nanofibers through dynamic imine chemistry enabled by dissolution-recrystallization process. Reproduced from [53] with permission from ACS.

2.2. COFs: Adsorption, storage and gas uptake applications

Ultrahigh accessibility, low crystal density, and rich-electronic network are suitable properties exhibited by the robust covalent organic COF-type frameworks, which would allow their efficient use for selective adsorption and gas storage. More specifically, the potential capacity of COF materials for H_2 storage has been predicted from theoretical studies using grand canonical Monte-Carlo simulated calculations. The results showed that around 10% of H_2 storage excess in COF-105 and COF-108 at 77 K, being the best known storage solids for molecular hydrogen at 77 K. The experimental H_2 loading data for COF-5, under conditions in which full evacuation of the pores was achieved, were 3.4 wt.% at 50 bar and 77 K. Moreover, the study revealed that the total H_2 uptake for COF-108 is 18.9 wt.% at 77 K, showing COF-102 the highest volumetric performance (40.4 g/L of H_2 at 77 K) (Fig. 22) [54].

These promising data were also confirmed for the storage of methane and carbon dioxide through isotherms carried out at 1-85 bar and 77-298 K of seven porous COFs. In function of the obtained uptake capacities, structural dimensions and pore sizes, the COFs materials were classified into three groups: (i) group 1 with 2D structures exhibiting 1D small pores (9 Å for COF-1 and -6), (ii) group 2 including 2D frameworks with large 1D pores (27 Å, 16 Å, and 32 Å for COF-5, -8, and -10, respectively), and (iii) group 3 with 3D architectures containing 3D medium-sized pores (12 Å for COF-102 and -103). Better adsorption results were achieved with group 3 than group 1 and 2, being the gas uptake comparable to the best metal-organic frameworks. This fact was corroborated by the gas uptake of COF-102 at 35 bar (72 mg/g at 77 K for H_2, 187 mg/g at 298 K for CH_4 and 1180 mg/g at 298 K for CO_2), being close to the results obtained for COF-103 but higher than those observed for COF-1, -5, -6, -8, and -10 (Fig. 23) [55]. In the specific case of methane uptake, the best material was COF-1, considering

total volume of CH_4 per unit volume of the COF absorbent. This stored 195 vol./vol. at 298 K and 30 bar, surpassing the objective of 180 vol./vol. at 298 K and 35 bar of the U. S. Department of Energy for CH_4 storage (Fig. 24). Simulations based on force fields indicated multilayer formation coexisting with a pore filling mechanism during the methane adsorption [56]. Definitively, these results clearly indicate that the COF systems are promising candidates like adsorbents for hydrogen, methane and carbon dioxide.

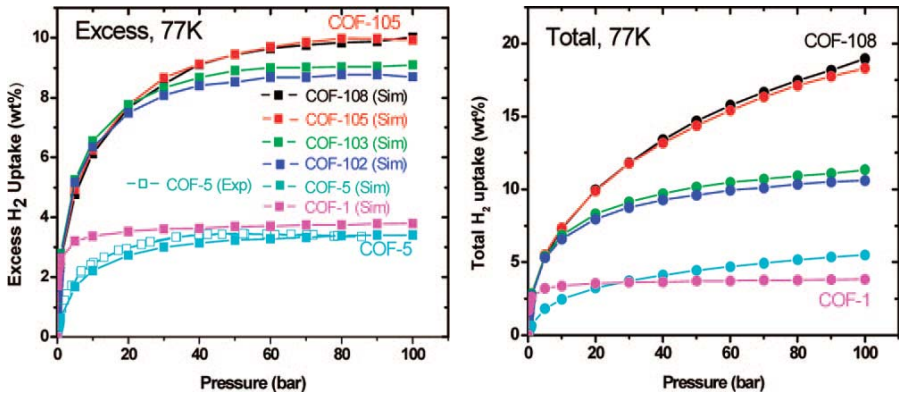

Figure 22. H_2 adsorption isotherms for COFs. Left: Excess H_2; Right: total H_2. Filled and open symbols show simulated and experimental data, respectively. Reproduced from [54] with permission from ACS.

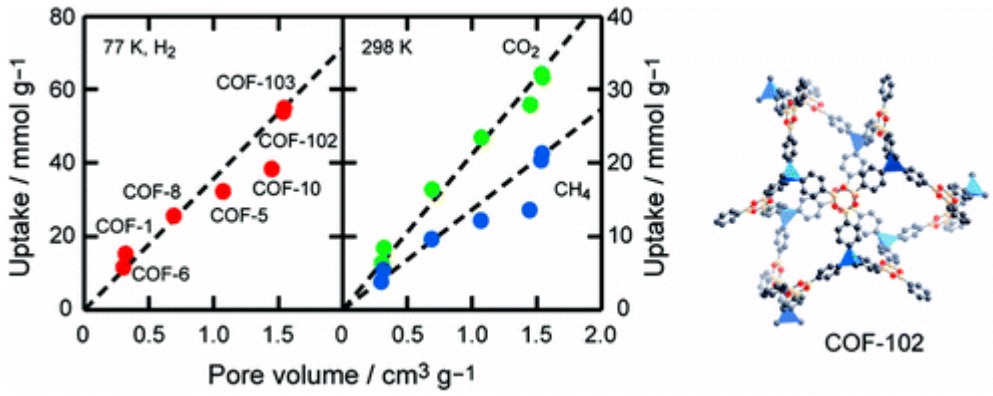

Figure 23. Comparison between gas uptake and pore volume of COFs calculated from Ar isotherms. Red, blue and green circles show gas uptake of H_2 (77 K, 70 bar), CH_4 (298 K, 70 bar), and CO_2 (298 K, 50 bar), respectively. Reproduced from [55] with permission from ACS.

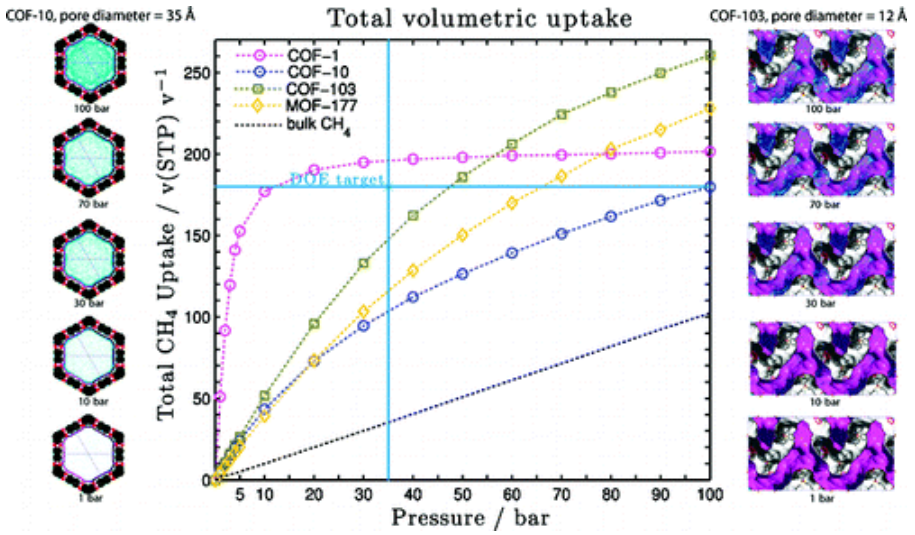

Figure 24. Predicted volumetric methane isotherms at 298 K for different COFs. The black dashed line indicates the uptake for free CH_4 gas. MOF-177 uptake is added for comparison. In the inset, ensamble average of methane molecules at different pressures for COF-10 and -103. Reproduced from [56] with permission from ACS.

Gas physisorption on porous materials is a promising way to achieve H_2 storage requirements for the transportation industry. This is due to adsorption-desorption is fast and fully reversible at mild conditions. However, the major part of current candidates lead to H_2 binding energies that are too weak, leading to volumetric capacities <10 g/L at 298 K, while the DOE 2015 marked objective is 40 g/L. The H_2 binding energy of 48 compounds based on different metalated analogs of five common linkers was studied using quantum mechanistic (QM) methods. Considering the first transition row metals plus Pd and Pt, the new COF-301-$PdCl_2$ achieved 60 g total H_2/L at 298 K and 100 bar, which was 1.5 times the DOE 2015 target and near to the recent fixed DOE 2050 target of 70 g/L. Meanwhile, promising MOF-200 and MOF-177 materials could store 7.6 g/L (0.54% excess) and 9.6 g/L (0.87% excess), respectively, at 298 K and 100 bar, unfavorably compared with 60 g/L (4.2% excess) for COF-301-$PdCl_2$ [57]. The insertion of Li alkoxide groups was also studied to enhance the H_2 storage ability of covalent organic framework materials. First-principles calculations predicted the structure of the Li alkoxide group in the COF-type materials and its effective interaction with multiple H_2 molecules, showing the increase of gravimetric and volumetric H_2 uptake both at 77 and 300 K and pressures up to 100 bar. Even, Li alkoxide COF achieved 22% and 51 g/L at 77K and 100 bar surpassing the DOE 2015 target for gravimetric uptake [58, 59]. Therefore, we can say that there are several theoretical studies which predict stronger interactions between different gases and the covalent organic frameworks (preferably metalated), which are to be experimentally validated.

The presence of abundant nitrogen sites in the structure of different COFs' families, such as those containing triazole, azine or imine linkages, could favor the adsorption capacity of small gas molecules and the separation processes. It is the case of CO_2 over N_2 and CH_4, probably due to the more favorable interaction of the nitrogen atoms located on the pore walls with polarizable molecules (CO_2) through dipole-quadrupole interactions [**38**, 60]. Another important variable to take into account in gas separation processes will be the porous topology exhibited by the COF materials. In this sense, microporous covalent organic framework, MCOF-1,with uniform pore sizes of 0.64 nm and synthesized from self-assembly of tetrahedral tetra(4-dihydroxyborylphenyl)methane (TBPM) with the linear 1,2,4,5-tetrahydroxybenzene (THB) under solvothermal conditions, showed high adsorption selectivity towards C_3H_8, C_2H_6 and C_2H_4 over CH_4. Specifically, to evaluate the gas separation ability of MCOF-1, it was calculated the C_3H_8/CH_4, C_2H_6/CH_4 and C_2H_4/CH_4 adsorption selectivities from ideal adsorption solution theory (IAST), at 298 K and 100 kPa [61]. The results obtained indicated that the C_3H_8/CH_4 selectivity for MCOF-1 is larger than 1800, for C_2H_6/CH_4 ~88 and C_2H_4/CH_4 ~26, ranking MCOF-1 among the best porous adsorbents for separating short (C2) hydrocarbons from CH_4, among zeolites, mesoporous organosilicas and MOFs (Fig. 25). The channels of the COF-1-type materials also allowed the efficient separation of hydrogen isotopes by quantum sieving after the inclusion of pyridine molecules into the free microporous cavities (Fig. 26) [62].

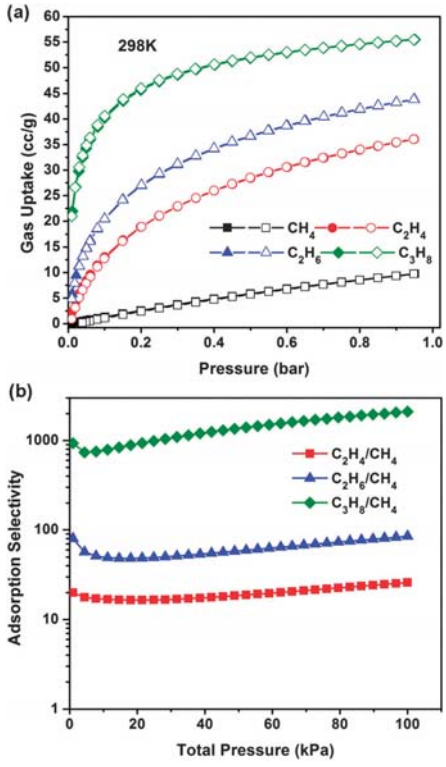

Figure 25. (a) Gas (black CH_4, red C_2H_4, blue C_2H_6 and olive C_3H_8) uptake isotherms of MCOF-1 at 298 K; (b) IAST predicted equimolar gas mixture adsorption selectivities for MCOF-1 (olive for C_3H_8/CH_4, blue for C_2H_6/CH_4 and red for C_2H_4/CH_4) at 298 K and 101 kPa. Reproduced from [61] with permission from RSC.

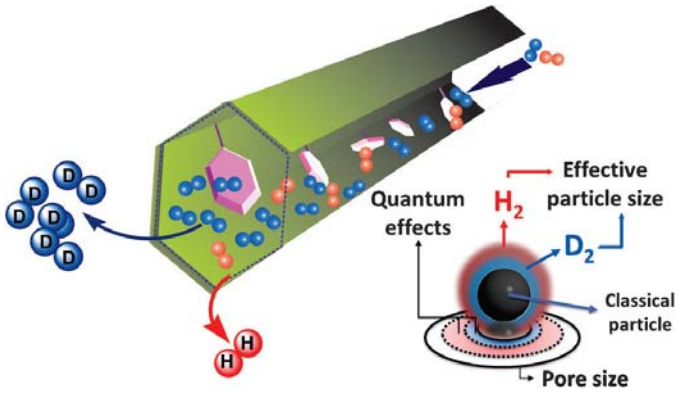

Figure 26. Pore channel of COF-1 with dangling pyridine molecules incorporated in the pore walls. The decreased size and the cryogenic flexibility of the aperture were employed for the enhancement of the quantum sieving effect for light isotopes. Reproduced from [62] with permission from Wiley.

Several COFs contain a high concentration of Lewis acid boron sites that strongly interact with Lewis basic guests, this phenomenon being interesting for the storage of damaging chemical compounds such as ammonia. This is the case of COF-10 that showed the highest ammonia uptake capacity (15 mol kg^{-1}, 298 K, 1 bar), comparing with microporous 13X zeolite (9 mol kg^{-1}), Amberlyst 15 (11 mol kg^{-1}) and mesoporous silica MCM-41 (7.9 mol kg^{-1}). Moreover, ammonia was eliminated of COF-10 by simple heating at 200 °C under vacuum. It was detected that repeated adsorption processes implied a modification in the interlayer packing, being lower its specific surface area for nitrogen adsorption. However, the ammonia uptake and the structural framework of the COF were maintained after several adsorption - desorption cycles due to the strong Lewis acid-base interactions (Fig. 27) [63].

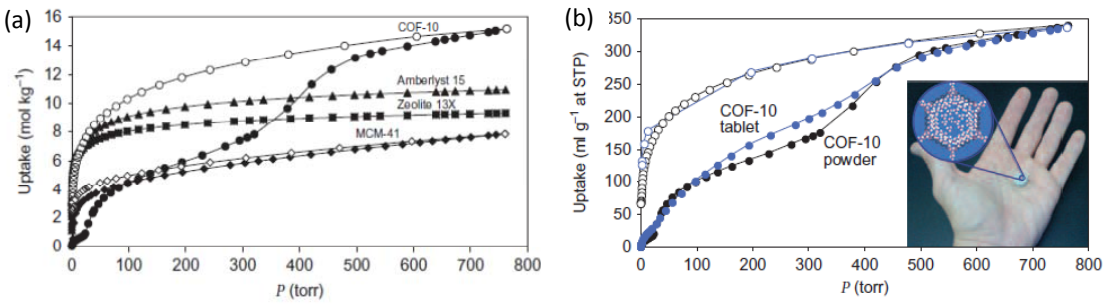

Figure 27. (a) Ammonia uptake at 298 K and 760 torr of COF-10 (15 mol kg^{-1}, circles), Amberlyst 15 (11 mol kg^{-1}, triangles), Zeolite 13X (9 mol kg^{-1}, squares) and MCM-41 (7.9 mol kg^{-1}, diamonds). Adsorption and desorption measurements correspond to closed and open symbols, respectively. (b) Ammonia

uptake at 298 K for COF-10 (black) and COF-10 tablet (blue). In the inset, tablet of COF-10 with adsorbed ammonia. Reproduced from [63] with permission from Macmillan Publishers.

2.3. COFs: Catalytic applications

2.3.1. C-C Bond forming reactions

COFs research lines have mainly been focused on the construction of novel ordered organic covalent structures with the aim of increasing the surface area and pore volume, seeking to improve gas uptake properties. However, their high stability towards hydrothermal treatments and most of the organic solvents, together with the possibility to incorporate catalytic active functions in the organic backbone suggests the possibilities of COFs for catalysis. The most conventional and well-known boron-containing COFs, linked by boroxine or boronate-ester groups, were unfortunately non-stable to polar media, although they exhibit high thermal stabilities. On the contrary, triazole-, imine- and hydrazone-based COF materials, being highly stable in water and in most organic solvents, show the minimal requirements to be used as catalysts. Moreover, it has been well demonstrated in coordination chemistry that the imine-type (Schiff base) ligands are versatile groups for incorporating a variety of active metal species. It is the case of COF-366 and COF-367 materials based on active cobalt porphyrin units connected through imine bonds with benzenedicarboxaldehyde linkers. These heterogeneous catalysts were effective for CO_2 reduction in water, achieving TONs up to 290000 with initial TOFs of 9400 h^{-1} [64].

These initial premises are the incentive to use imine-linked metal-ion-incorporated COF materials for catalysis. Specifically, the imine-linked COF-LZU1 presents a two-dimensional eclipsed layered-sheet structure, where the incorporation of stabilized metal ions is possible. As consequence, the Pd(II)-containing COF, named as Pd/COF-LZU1, was synthesized by post-synthesis treatments, showing excellent catalytic activity (yields of 96-98%), high stability and easy recyclability for the Suzuki-Miyaura coupling reaction, an important reaction for the formation of C-C bonds. In comparison with other crystalline porous materials (zeolites and MOFs), the unique structure of Pd/COF-LZU1 provided efficient access to the catalytic sites and fast mass-transport of the reactants/products, being this fact responsible for its superior catalytic activity. Specifically, the eclipsed layered-sheet arrangement of COF-LZU1 offered a robust scaffold for $Pd(OAc)_2$ incorporation and the distance (~3.7 Å) of eclipsed nitrogen atoms in adjacent layers fell into the ideal requirement for strong coordination of $Pd(OAc)_2$. Moreover, the regular channels with a diameter of ~1.8 nm provided efficient access to the active sites together with fast diffusion for the bulky products (Fig. 28) [65].

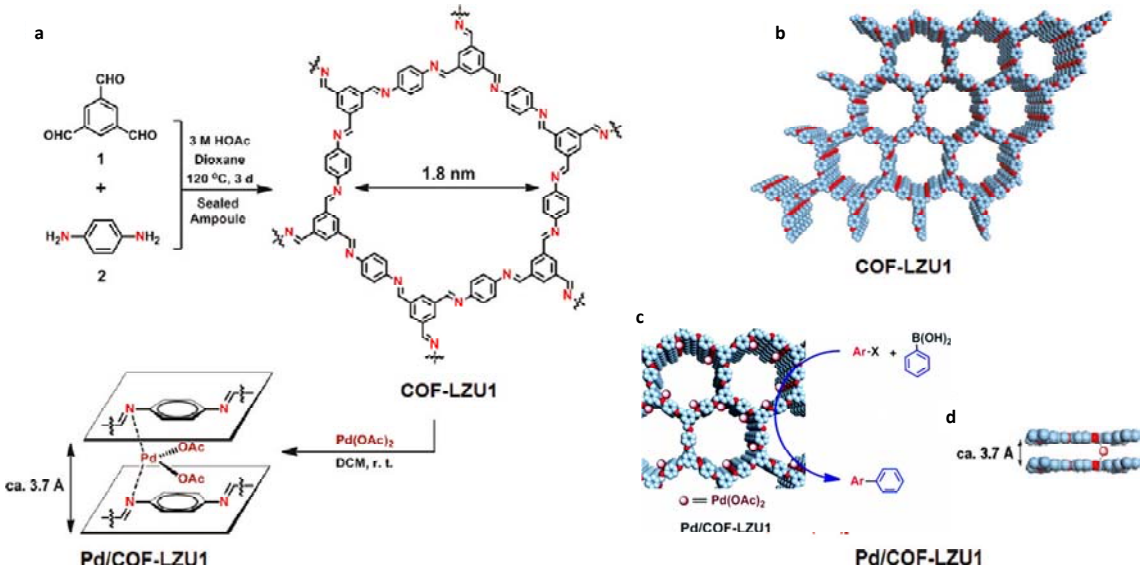

Figure 28. Construction of COF-LZU1 and Pd/COF-LZU1. (a) Representation for the synthesis of COF-LZU1 and Pd/COF-LZU1 materials. Proposed structures of (b) COF-LZU1 and (c,d) Pd/COF-LZU1, exhibiting homogeneous microporous channels (diameter of~1.8 nm). Brown spheres indicate $Pd(OAc)_2$. Inset in (c) with the reaction scheme of Suzuki-Miyaura coupling reaction. Reproduced from [65] with permission from ACS.

Highly dispersed Pd(0) nanoparticles were also successfully immobilized into stable, crystalline and porous covalent organic framework, so-called TpPa-1, by a solution infiltration method using $NaBH_4$ as reducing agent. High resolution and dark field TEM images confirmed the uniform loading of the Pd(0) nanoparticles into the TpPa-1 network without apparent aggregation. This hybrid material showed excellent catalytic activity towards the Cu-free Sonogashira, Heck, and sequential one-pot Heck-Sonogashira cross-coupling processes under basic conditions, exhibiting better catalytic behavior than commercial available Pd nanoparticles supported on activated charcoal. Moreover, Pd(II) complex doping COF matrix also showed high catalytic activity for the intramolecular oxidative biaryl synthesis under acidic conditions. Both types of Pd-COF catalysts were highly stable under the reaction conditions, exhibiting unappreciable metal leaching without aggregation and good recyclability. Thus, TpPa-1 represented the first COF material that can support both Pd(0) nanoparticles and Pd(II) complexes without aggregation for several catalytic reactions under highly acidic or basic conditions, with competitive performances (Fig. 29) [66].

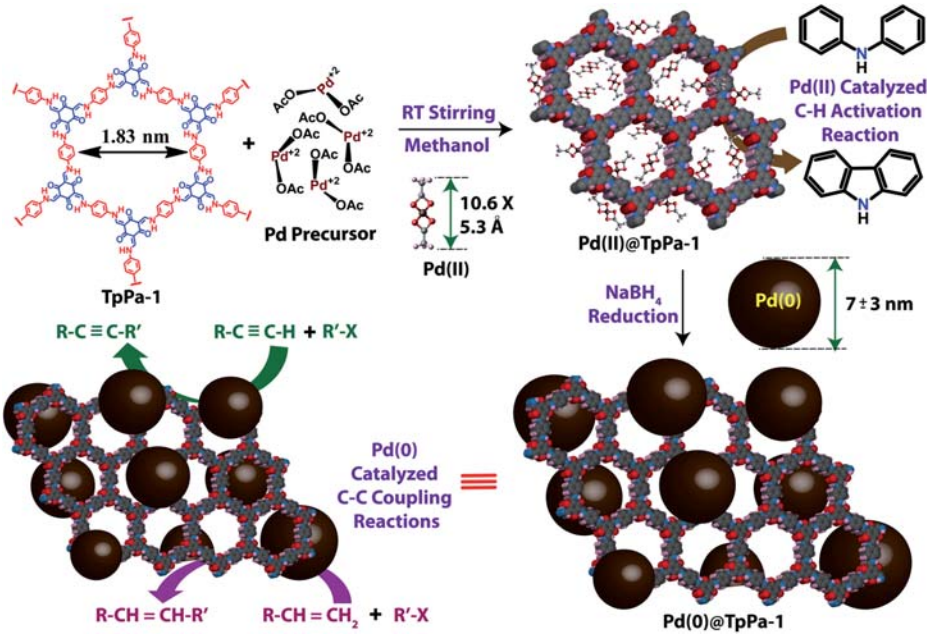

Figure 29. Preparation of Pd (II) and Pd (0)-doped COFs (*i.e.,* Pd(II)@TpPa-1 and Pd(0)@TpPa-1) and their use as catalysts for the Sonogashira, Heck and oxidative biaryl coupling reactions. Reproduced from [66] with permission from RSC.

Similarly, Au(0) nanoparticles (~5 nm) were also immobilized into TpPA-1 COF material, used as support, through infiltration procedure. The as-synthesized Au(0)@TpPa-1 catalyst showed higher reusability and activity for nitrophenol reduction than $HAuCl_4 \cdot 3H_2O$. Specifically, the reaction did not occur when using only TpPa-1 as catalyst and was slower with $HAuCl_4.3H_2O$ and Au(0)@TpPa-1 (2.20 wt%) as catalysts. However, when 1.2 wt% Au was present in the Au(0)@TpPa-1 catalyst, relevant catalytic activity was observed and conversion of 4-nitrophenol to 4-aminophenol was completed in 13 min (Fig. 30). A possible explanation for the observed catalytic behavior can be the homogeneous distribution of tiny nanoparticles (5 ± 3 nm) on the TpPa-1 support, which implied a high surface area of the nanoparticles accessible to reactants [67].

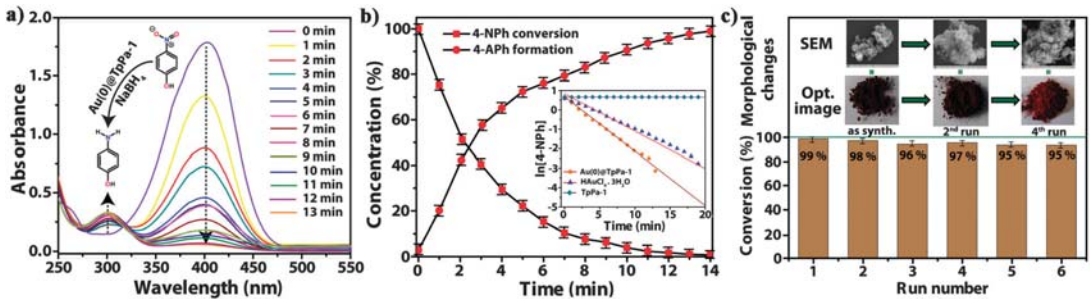

Figure 30. (a) Time-dependent evolution of UV-vis spectra, reflecting the catalytic reduction of 4-nitrophenol to 4-aminphenol by Au(0)@TpPa-1. (b) Kinetics of the reduction reaction. (c) Conversion of

4-nitrophenol for 6 cycles of reaction by the Au@TpPa-1 catalyst. Reproduced from [67] with permission from RSC.

2.3.2. Oxidation processes

The catalytic results showed above indicate that the nitrogen-rich COFs, containing frameworks based on imine-linkages, exhibited excellent properties to be used as matrix supports of metallic nanoparticles or organometallic complexes. Similar tendency was observed with COFs based on hydrazine linkages where accessible molybdenum-doped covalent organic framework catalyst (Mo-COF) was obtained from two-step bottom-up approach, being catalytically active for selective oxidation reactions, such as epoxidation of alkenes (cyclohexene, cyclooctene, styrene and *iso*-propenylbenzene). In this case, Mo sites were ordered into the channel walls of π-arrays of hydrazine backbone, through robust coordination between molybdenyl acetylacetonate ($MoO_2(acac)_2$) and the π-connected benzoyl salicylal hydrazone ligand, forming an effective nanochannel-reactor (Fig. 31). This approach allowed the easy access of guest molecules through the 1D channel to the anchoring sites. Based on these structural characteristics, the corner unit of this COF was involved in two different roles: connecting the building blocks and providing free positions for loading Mo sites. The high selectivities achieved showed that this novel nanochannel-reactor exhibited a typical porous structure of two-dimensional COF, providing a desirable micro-environment for selective oxidation reactions [68].

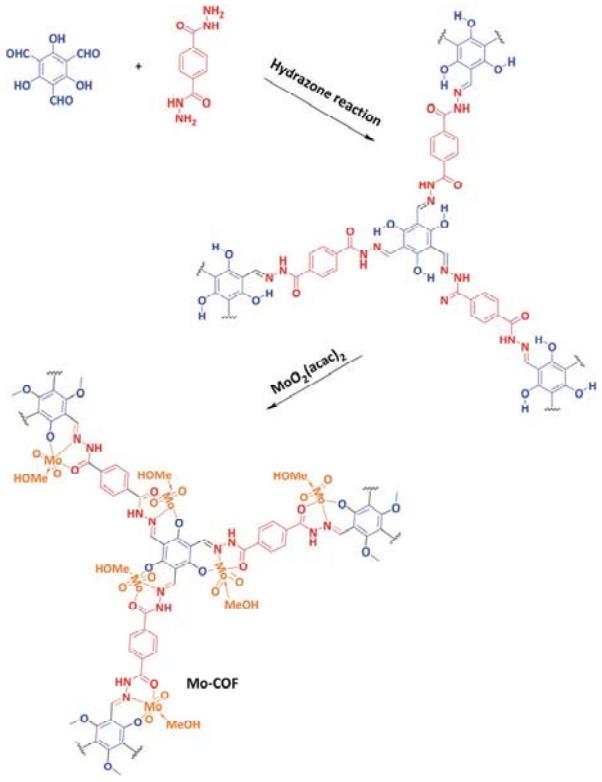

Figure 31. Formation of the molecular building blocks of Mo-COF, favoring the formation of catalytic active sites. Reproduced from [68] with permission from RSC.

2.3.3. Catalytic processes using post-modified COFs: Chiral COFs

Different pathways were used to incorporate accessible functionalities into the pores of organic frameworks to obtain active COFs-type catalysts. One of them is the pre-functionalization of monomers used as building blocks. In this sense, carboxylic acid groups were introduced onto the pore walls of COF-30, a two-dimensional hexagonal COF, through the pre-polymerization modification of the bis-diol monomer, 1,2,4,5-tetrahydroxybenzene, used during the solvothermal synthesis process [69]. Another procedure was the post-functionalization of previously synthesized COF structures to incorporate active functions into the porous organic framework, generating novel catalysts' families. Following this approach, truncation-functionalization strategy was useful to introduce additional active sites. This is the case for as-synthesized truncated 3D COF-102 that contains allyl groups in the pore walls which were involved in thiol-ene coupling reactions, preserving the crystallinity and porosity of the pristine framework (Fig. 32). This approach can be a potential route to obtain stable COFs catalysts through the post-modification of organic linkers which form the structure [70]. In fact, recently, chiral organocatalysts were incorporated through post-synthesis treatments of 2D imine-based COFs by azide-ethynyl click reactions. The result was the presence of homogeneously distributed *(S)*-pyrrolidine moieties pending from organic walls to free porous channels. The recyclable chiral COF was active for asymmetric Michael reactions with different β-nitrostyrene derivatives, achieved conversions of 100% in six hours with *ee* of ~95% for chlorosubstituted substrates [71]. This latter example opens the possibilities to generate active heterogeneous chiral catalysts based on COFs.

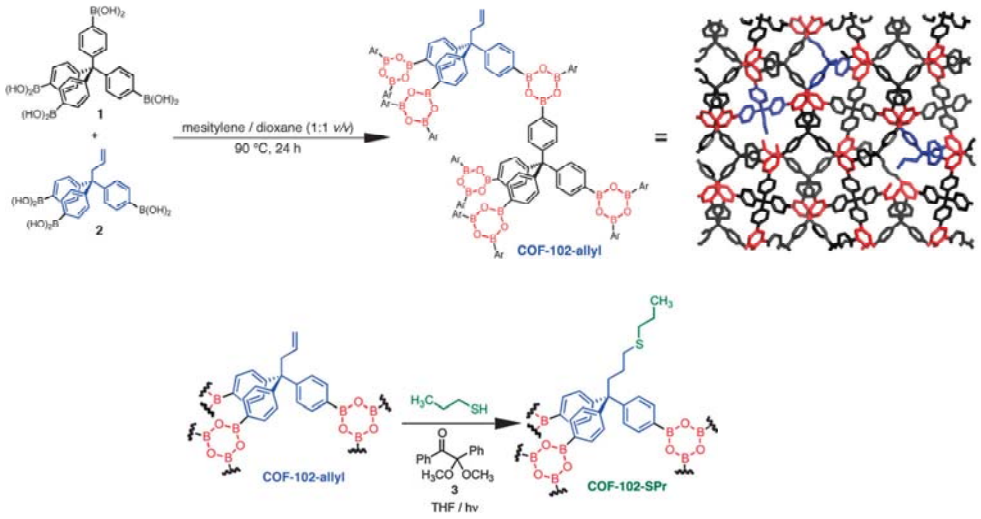

Figure 32. Co-crystallization of COF-102 derivatized with allyl groups. COF-102-allyl was involved in thiol–ene conditions to generate COF-102-SPr. Reproduced from [70] with permission from RSC.

2.3.4. Photocatalytic reactions

The COF structures, based on ordered porous polymers networks combining robustness and molecular functionality with the possibility to incorporated doping metallic species, favor the generation of effective photocatalysts. It is the case of new COF materials useful for visible-light driven hydrogen production in presence of Pt as proton reduction catalyst (PRC). Specifically, this COF was constructed through hydrazone-linkages functionalized with triazine and phenyl building blocks, forming a lamellar structure with a honeycomb-type architecture with mesopores of 3.8 nm. When the suitable organic solid was illuminated with visible light, the Pt-loaded COF continuously produced hydrogen from water without structural degradation. So, photoactive COFs are well-defined model systems to carry out efficiently photocatalytic processes (Fig. 33) [72].

In fact, COF structures based on π-conjugated backbones, with high surface area and abundant 2-dimensional hetero-interface, emphasize their use as effective supporting matrixes for stabilizing generated photoelectrons with high photocatalytic activities. This behavior was confirmed when CdS nanoparticles were deposited on a highly stable 2D COF matrix, and the generated hybrid nanocomposite was used as a photocatalyst for visible-light-driven hydrogen production (Fig. 34). Particularly, the efficiency of CdS-COF hybrid was studied by varying the COF content. On the introduction of only 1% of COF, a 10-fold increase in the overall photocatalytic activity of the hybrid was measured, exhibiting a marked H_2 production around 3700 μmol h^{-1} g^{-1} when 10% COF content was present in the hybrid photocatalyst, which was significantly higher than for bulk CdS particles (124 μmol h^{-1} g^{-1}) [73].

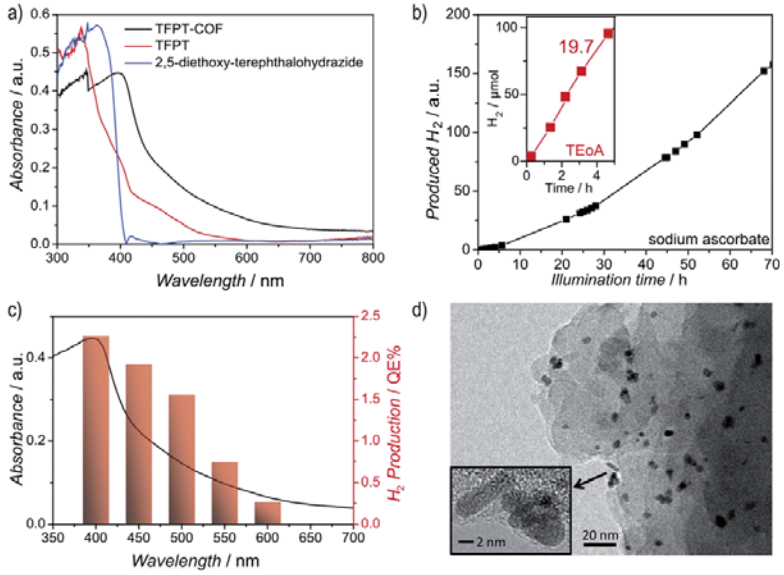

Figure 33. Optical properties of the TFPT–COF and photocatalytic hydrogen evolution. (a) UV/Vis diffuse reflectance spectra of TFPT–COF (black) and its monomers (blue and red). (b) Time course of hydrogen evolution by the Pt-modified TFPT–COF under visible light irradiation (I > 420 nm). The inset shows the

hydrogen evolution rate (19.7 mmol h^{-1}). (c) UV/Vis absorption of TFPT–COF and wavelength-specific hydrogen production of Pt-modified TFPT–COF. (d) TEM image of TFPT–COF/Pt after illumination for 84 h, showing the formation of Pt nanoparticles (5 nm). Reproduced from [72] with permission from RSC.

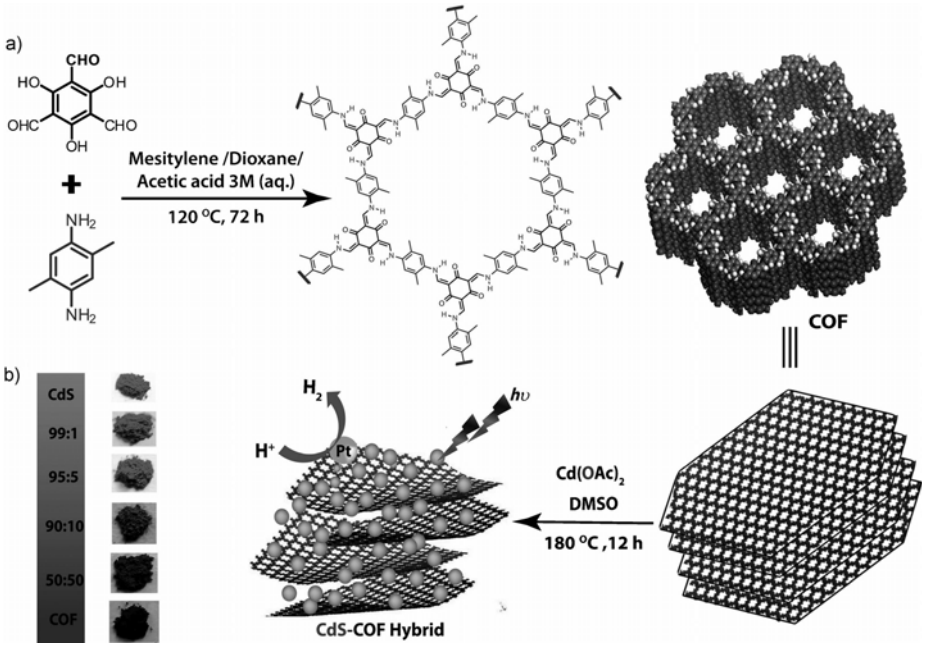

Figure 34. Representation of (a) synthesis of the covalent organic framework (COF) TpPa-2 and (b) CdS-COF hybrid formation by CdS nanoparticles incorporation on the COF matrix. Reproduced from [73] with permission from Wiley.

2.4. COFs: Applications for nanotechnology

2.4.1. Electronic and photovoltaic applications

In general, COF-type covalent organic structures are characterized by rich-electron frameworks together with the presence of photoluminescent units inserted onto the walls. These properties enhance the potentiality of COFs for nanotechnological applications related with conducting, sensoring, imaging or optoelectronic devices. It is the case of COFs with architectures based on covalently linked porphyrin moieties. These crystalline solids were formed by nanosheets in which the porphyrin groups were stacked laterally to give an efficient conducting interface. Specifically, COF-366 and COF-66 were determined to be hole conducting with mobilities as high as 8.1 and 3.0 $cm^2 V^{-1} s^{-1}$. So, these multifunctional conducting organic materials combine thermal stability, electrical conductivity, high charge mobility and elevated pore accessibility, representing an important alternative for designing realistic plastic electronics, optoelectronic systems and type solar cells with longer lifetimes [74].

Charge dynamics were also detected in donor-acceptor COFs with homogenously distributed bi-continuous heterojunctions, using time-resolved spectroscopy to elucidate photochemical processes of the free charges, from their generation to delocalization and

retention. In the as-synthesized COFs materials, the heterojunctions allowed an ultrafast electron transfer from the donor to the acceptor columns, being the light absorption directly coupled with charge dissociation to favor free charges in the donor and acceptor π-columns. Furthermore, the stacked π-columns delocalized the charges, suppressed charge recombination and retained the charges for a prolonged period. In detail, this specific donor-acceptor material was a tetragonal, mesoporous 2D COF that was formed by Zn phthalocyanine electron-donor and naphthalene diimide acceptor units. Interestingly, the COF provided self-sorted bi-continuous columnar arrays and formed periodically structured heterojunctions in which each donor column was interfaced with four acceptor columns that were active to capture photogenerated electrons (Fig. 35) [75].

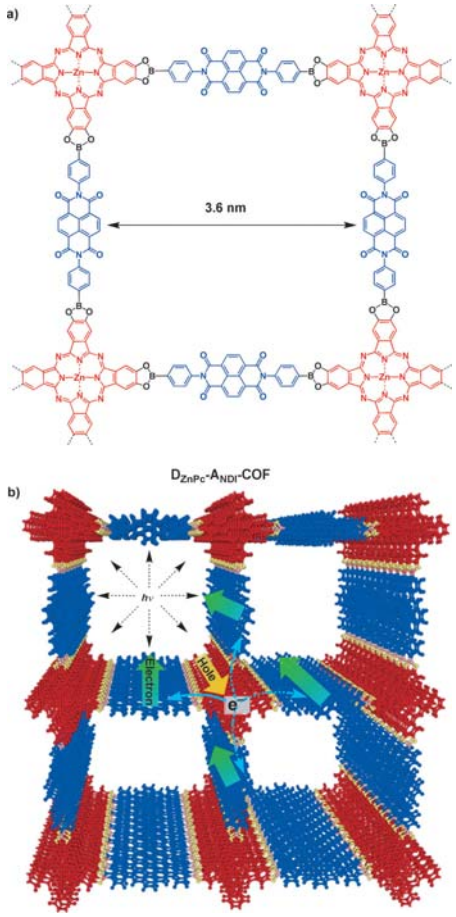

Figure 35. (a) Donor–acceptor COF (D_{ZnPc}-A_{NDI}-COF). Donor and acceptor units are shown in red and blue, respectively. (b) Representation of a 2x2 cell of the 0.8 Å slipped AA-stacked COFs and photochemical processes scheme. Reproduced from [75] with permission from Wiley.

New interpenetrated COF materials, where the distance between donor sub-networks and acceptor phases are also present, were detected in photoconductive thienothiophene (TT) COF materials which showed charge transfer towards included fullerene. This structure supported efficient charge transfer within the lifetime of the excitons, showing that charge-

separation was possible with this system. Thus, interpenetrated frameworks of crystalline semiconductor COFs with electron acceptor moieties, such as fullerene [6,6]-phenyl-C_{61}-butyric acid methyl ester (PCBM), are promising networks to be used as effective photovoltaic devices for solar cells (Fig. 36) [76, 77].

Alternatively, proton conducting COF-type materials were also prepared through the immobilization of H_3PO_4 acid within the porous organic frameworks based on keto-enamine linkages, facilitating the proton conduction both in hydrous ($\sigma = 9.9 \times 10^{-4}$ S cm^{-1}) and anhydrous states ($\sigma = 6.7 \times 10^{-5}$ S cm^{-1}). In this case, two stable functional crystalline COFs (Tp-Azo and Tp-Stb) were doped with acid molecules which were synthesized using the Schiff base reaction between triformylphloroglucinol (Tp) and 4,4'-azodianiline (Azo) or 4,4'-diaminostilbene (Stb), respectively (Fig. 37) [78].

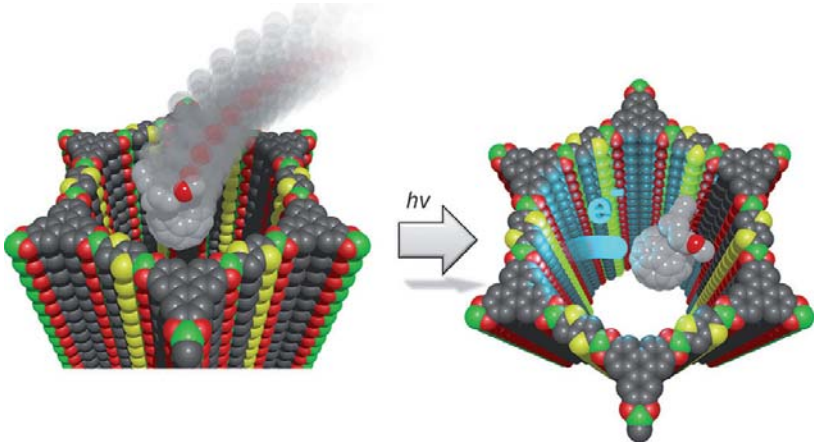

Figure 36. Scheme of the host–guest complex of TT-COF and PCBM molecule (Carbon: grey; Oxygen: red; Boron: green; Sulfur: yellow). Reproduced from [76] with permission from Wiley.

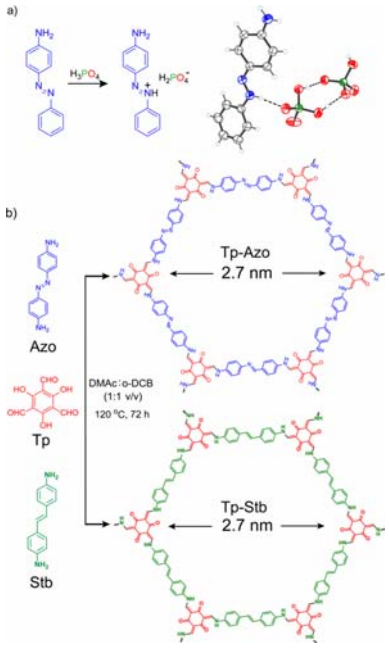

Figure 37. (a) Crystal structure of 4-[(E)-phenyl-diazenyl]anilinium dihydrogen phosphate. (b) Synthesis representation of Tp-Azo and Tp-Stb materials. Reproduced from [78] with permission from ACS.

However, although it is possible to synthesize π-conjugated COF systems with high conductivities and charges' separation, their intrinsic rigidity and poor handling processability seriously limit their applications in flexible electronics devices. Thus, the preparation of high charge-carrier COF materials as flexible and versatile thin films is an important challenge in materials' science. Advances into this topic are related with the growth of oriented thin films of tetrathiafulvalene-based COF materials (TTF-COF). They allowed the diffusion of dopants such as I_2 and tetracyanoquinodimethane (TCNQ) for redox reactions, while closely packed 2D grid sheets facilitated the cross-layer delocalization of TTF radical cations, generating more conductive mixed-valence TTF species (Fig. 38). In this case, conductivities as high as 0.28 S m^{-1} were estimated for the doped TTF-COF thin films, being among the highest up to now reported for COF-type solids [79, 80].

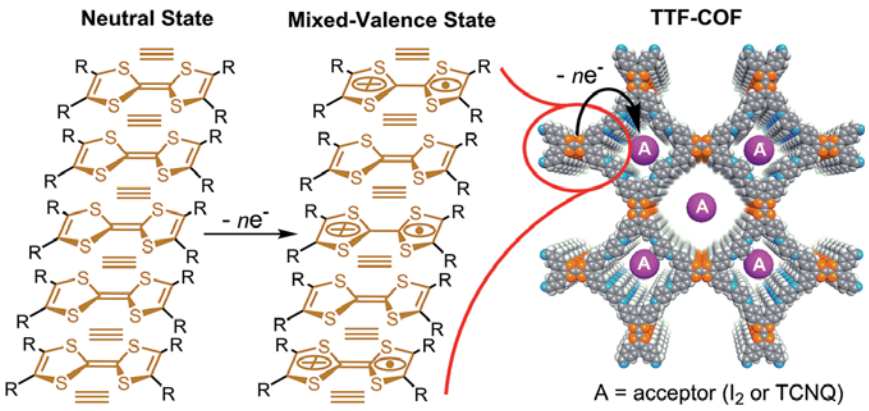

Figure 38. Representation of the mixed-valence state in TTF-COF. Reproduced from [80] with permission from RSC.

Following this line, electron-donor oriented mesoporous COFs synthesized as thin films (BDT-COF) were prepared from assembly of a benzodithiophene-diboronic acid and hexahydroxytriphenylene (HHTP) through synthesis-deposition on different polycrystalline surfaces (Fig. 39). Additionally, thin BDT-COF films were doped with fullerene compounds (as PCBM above commented) to produce interpenetrated electron-donor/acceptor host-guest COF materials. Light-induced charge transfer phenomenon from BDT-COF to PCBM acceptor moieties was corroborated through the efficient photoluminescence quenching. This study showed the potentiality of thin COF-type films as ordered porous materials in which combined

structural and optical properties are suitable for the development of electron-donor and electron-acceptor device components [81, 82].

Relevant advances have been achieved in the generation of COF-type thin films as photovoltaic devices where the donor and acceptor units were not separated, but forming one-dimensional stacks extended along the framework, favoring a suitable spatial arrangement for charge transport. In this case, heterojunction as active layer was exclusively forming the crystalline COF based on triphenylene and porphyrin units (Fig. 40) [83].

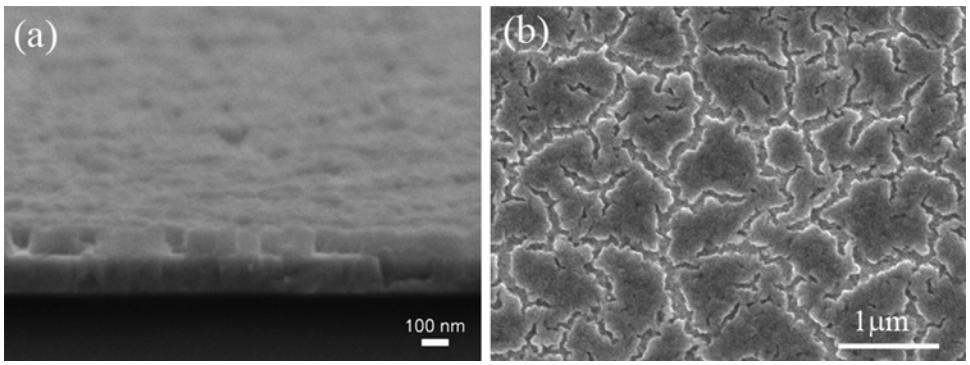

Figure 39. (a) SEM micrograph in cross section and (b) in top view of BDT-COF thin film grown on an ITO-coated glass substrate. Reproduced from [81] with permission from ACS.

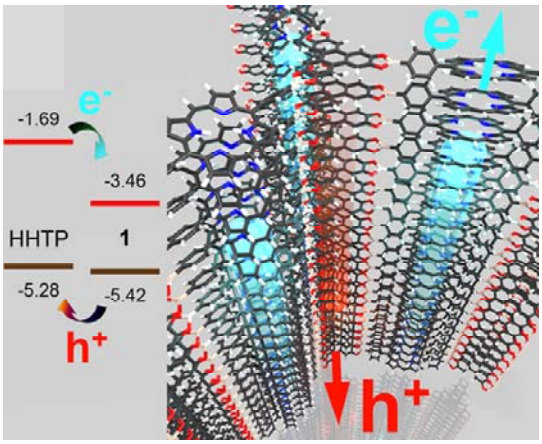

Figure 40. Frontier orbital energies of the two COF subunits measured by differential pulse voltammetry (DPV) together with scheme of the photoinduced charge transfer. Reproduced from [83] with permission from ACS.

The potentiality exhibited by the directly synthesized and grown COF thin films on single-layer graphene (SLG) for their incorporation in purely organic optoelectronic devices is remarkable. In this case, under solvothermal conditions, the formed layered films showed improved crystallinities compared with more conventional COF powders, using SLG surfaces incorporated on copper, silicon carbide, and transparent fused silica (SiO_2) as stable supports. Moreover, through combined studies from scanning tunneling microscopy and DFT theoretical simulations, the strong coupling and vertical alignment established between the COF surface,

structured by Schiff base network, and single-layer graphene was corroborated (Fig. 41) [84,85,86]. In addition, electronic properties of COF thin films grown on graphene were studied using dispersion-corrected DFT methods. The results showed that aromatic central builder units of the COF frameworks acted as electron-donor to graphene, while the linker was as an electron-acceptor, being the interaction between the filled orbitals of the central aromatic units and empty orbitals of the linkers decisive to favor the formation of planar COF networks on graphene [87].

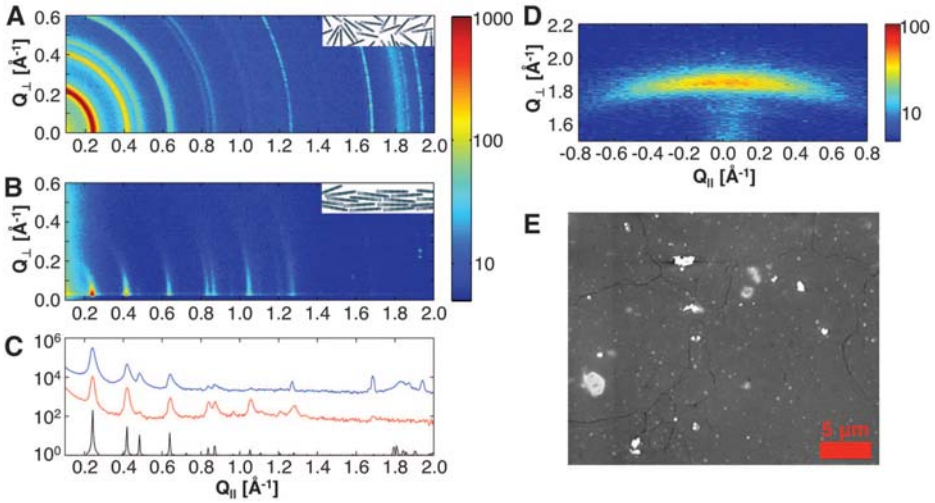

Figure 41. (a) X-ray scattering data obtained from COF-5 powder; (inset) scheme of randomly oriented COF-5 grains in the powder, as indicated in (a). (b) Grazing incidence diffraction (GID) data from a COF-5 film on SLG/Cu; (inset) scheme of oriented COF-5 grains in the film, as indicated in (b). (c) Projections of (a) (top/blue) and (b) (middle/red) and the simulated powder diffraction spectrum (bottom/black) for COF-5. (d) GID data, showing an off-specular projection of the COF-5 film (001) Bragg peak. (e) Top-down SEM image of the COF-5 thin film studied in (b), (c), and (d). Reproduced from [84] with permission from Science eds.

2.4.2. Photoluminiscent applications: Sensors

Concerning luminescent potential applications, fluorescent nanoparticles of a novel type of melamine COF-type porous architecture, so called SNW-1, which was obtained through rapid microwave-assisted approach, was used as effective sensoring material. The as-synthesized SNW-1 nanoparticles exhibited high sensitivity and selectivity, as well as fast response to nitroaromatic explosives, such as 2,4,6-trinitrotoluene (TNT), 2,4,6-trinitrophenylmethylnitramine (Tetryl) and picric acid (PA) [88]. Furthermore, the incorporation of pyrene and triphenylene units by solvothermal polymeric condensation favored the formation of belt-shape hexagonal mesoporous COFs, which exhibited photonic absorption, emitting blue luminescence and acting as semiconducting material (Fig. 42) [89]. The self-condensation of pyrenediboronic acid allowed the crystallization of 2D COF materials

based on aligned polypyrene sheets in micrometer-scale cubes. This spatial distribution of uniform nanolayers facilitated exciton migration and carrier transportation. This polypyrrole COFs exhibited visible light harvesting and photocurrent production with a fast response to irradiation with visible light, without apparent structure deterioration (Fig. 43) [90]. In the same line, 2D COFs with pyrene units occupying structural vertices and diazabutadiene (-C=N-N=C-) moieties located in edges of rhombic sheets, favored the formation of AA-stacking modes to form periodically ordered pyrene columns and 1D microporous channels. Owing to pyrene columnar ordering, the azine-connected networks were highly luminescent, whereas the azine fragments were useful as open anchoring points for hydrogen-bonding interactions. These cooperative functions located on vertices and edges allowed the use of this pyrene-COFs as chemosensors for the detection of explosive molecules such as 2,4,6-trinitrophenol [**30**].

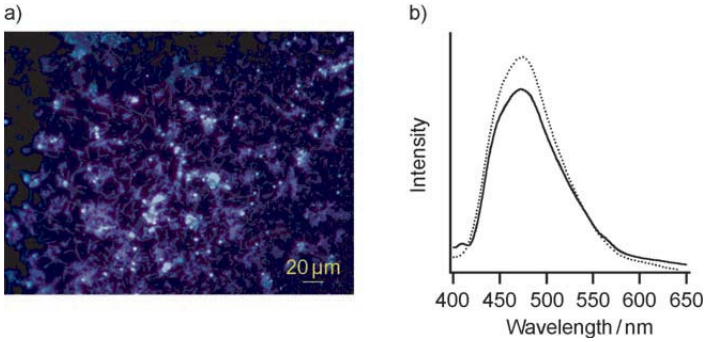

Figure 42. (a) Fluorescence image of TP-COF. (b) Fluorescence spectra of TP-COF upon excitation at 340 nm (black curve) and 376 nm (dotted curve) at 25 ºC. Reproduced from [89] with permission from Wiley.

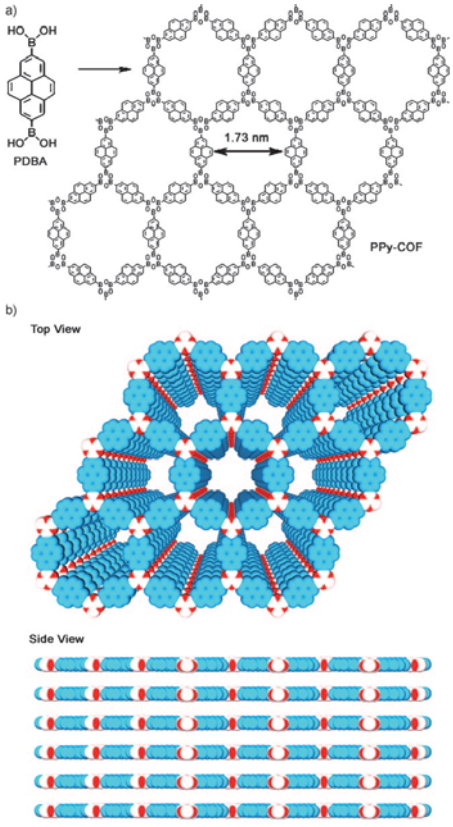

Figure 43. Scheme of (a) preparation and (b) structure of PPy-COF. (Boron: white; Oxygen: red; pyrene: blue). Reproduced from [90] with permission from Wiley.

Blue luminescent two-dimensional layered COFs were studied through theoretical time-dependent density-functional tight-binding (TD-DFTB) method, showing the importance of the interlayer spacing in the optical properties. The results suggested that adjacent layers were considerably more stable if their stacking arrangement was horizontally offset by approximately 1.4 Å compared with the eclipsed AA-stacking structure, showing the low-symmetry offset stacking higher luminescence intensity but lower carrier transport capacity. These computational calculations are useful to the optimal designing of optoelectronic devices based on 2D COF materials [91].

3. Porous Aromatic Frameworks: PAFs

3.1. PAFs: Synthesis, structure and properties

3.1.1. PAFs obtained through coupling reactions

Within covalent porous structures based on the effective assembly of organic building blocks, periodic aromatic frameworks (PAFs) occupy a predominant position, and the number of studies published in the last years focused on this type of organic materials is growing. Compared with the more conventional COFs obtained by reversible condensation chemistry routes, the PAFs-type solids are prepared through irreversible cross-coupling reactions generating more stable and robust materials, although with higher irregular internal structure that reduces their porosity and associated crystallinity. This latter characteristic connects PAFs with traditional rigid porous organic polymers, such as porous polymer networks (PPNs), conjugated microporous polymers (CMPs) and element-organic frameworks (EOFs), which share the same irregular and tortuous internal structure due to the nature of the bond-forming chemistry [**16**].

PAFs materials are constructed by exclusively aromatic rigid linkers, acting as organic builders, which are directly self-assembled under catalyzed solvothermal synthesis conditions. This assembly was established by tetrahedrally connected carbon atoms as covalent attachment points. Actually, the original idea for the synthesis of PAFs came from the structure of diamond, in which each carbon atom is tetrahedrally connected to four neighboring atoms by covalent bonds. Breaking the C–C covalent bond of diamond and inserting rigid aromatic rings, the formation of ordered organic structures is allowed. The obtained PAF materials exhibits more robustness and physico-chemical stability than, in general, previous revised COFs materials, together with significant crystallinity and accessibility [**14**]. This synthesis'

strategy opened a novel pathway for the preparation and construction of porous solids with enhanced hydrothermal stabilities for catalysis, adsorption, clean energy and environmental applications. Following this idea and with the support of computational studies, porous aromatic framework, so-called PAF-1, with high Langmuir specific surface area of 7100 m^2g^{-1} was obtained through the nickel (0)-catalyzed Yamamoto-type Ullmann cross-coupling reaction from tetrakis(4-bromophenyl) methane. This solid exhibited local diamond-like tetrahedral bonding of tetraphenylenemethane building units, showing exceptional thermal and hydrothermal stabilities (Fig. 44) [92]. In addition, modeling studies using amorphous silica models as template confirmed that tetrahedral node-to-node distance in PAF-1 structure was long enough to achieve high degree of microporosity, but not sufficient for interpenetration or formation of mesoporous network [93]. Furthermore, theoretical formation mechanism studies through an automated generation process evidenced the importance of the solvent in the resulting PAF-1 structure and their associated textural properties [94].

The same diamond topology as PAF-1 but with four aromatic rings as tetrahedral unit was achieved in the PAF-11 material *via* Suzuki cross-coupling reaction, using diboronic acid as linker. In this case, theoretically, the pores of PAF-11 should reach mesoporous size, being this fact corroborated by experimental characterization results, exhibiting surface area around of 950 $m^2\ g^{-1}$ in the Langmuir model and 700 $m^2\ g^{-1}$ in the BET model. Moreover, PAF-11 showed high chemical stability, maintaining its structure after treatments with different solvents or concentrated hydrochloric acid solutions [95].

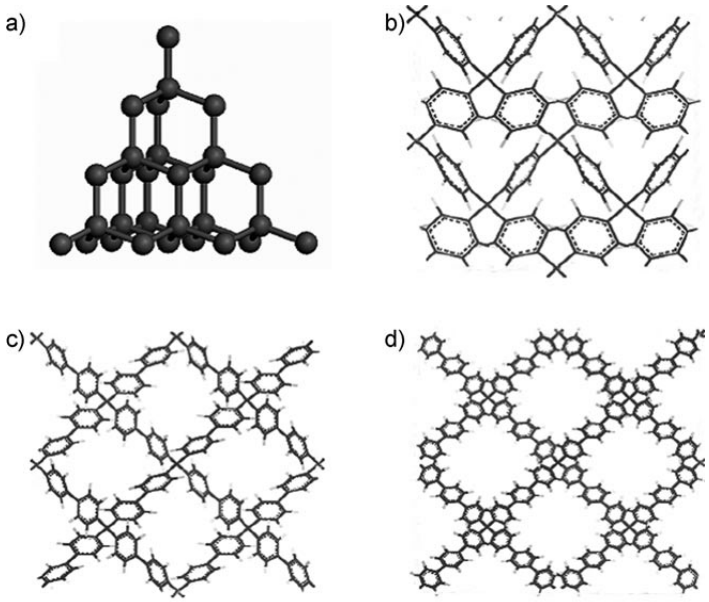

Figure 44. Representations indicating the replacement of the C-C bond in the diamond ideal structure (a) with one (b), two (PAF-1) (c) and three phenyl rings (d). Reproduced from [92] with permission from Wiley.

Ionothermal conditions were used to obtain PAF-2 material based on the suitable trimerization of building tetrakis(4-cyanophenyl)methane monomers catalyzed by $ZnCl_2$. In this case, three aromatic nitrile groups were trimerized to form a C_3N_3 triazine ring which connected with tetraphenylmethane units through covalent bonds to form a 3D porous organic framework. Figure 45 shows *ctn* and *bor* networks built up by fitting both tetrahedral (tetraphenylmethane) and triangular (C_3N_3 ring) building units on the corresponding structural nodes [96]. On the other hand, PAF-16 solid was structurally analogous to PAF-2, although during the synthesis was selected tetrakis(4-cyanophenyl)silica (TCPSi) as polymerization monomer because the synthesis can be performed in safer conditions than using tetrakis(4-cyanophenyl)methane (TCPM) without modifying substantially the formed network [97].

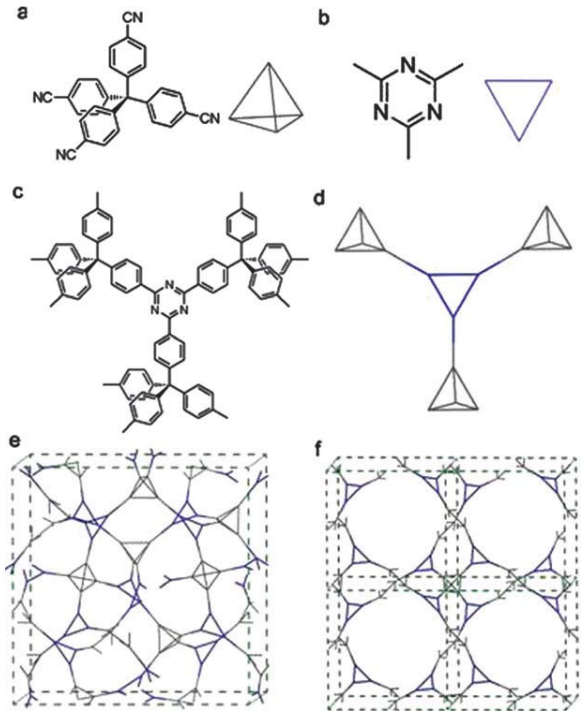

Figure 45. Synthesis of PAF-2 material based on assembly of tetrakis(4-cyanophenyl)- methane (a) and planar triangular C_3N_3 ring (b) through trimerization process. A secondary building unit is formed by connecting three tetrahedral units with the planar triangular ring, (c) and (d). These building units linked together generate the swelled *ctn* (e) and *bor* (f) nets, respectively. Reproduced from [96] with permission from RSC.

Advancing in the synthesis of novel PAF-type materials, homocoupling of tetrahedral phenyl monomers with adamantane cores was also effective to synthesize porous polymer networks (so-called PPNs), through oxidative Eglinton coupling of terminal alkynes besides the Yamamoto reaction. However, although non-interpenetrated diamondoid frameworks were obtained, these hydrophobic hyper-crosslinked polymers exhibited high thermal and chemical stabilities (Fig. 46) [98].

Other types of planar aromatic monomers have been used as building units to generate further PAFs structures. It is the case of the solids based on spirobisfluorene fragments obtained by combining 1,4-benzenediboronic acid with tetra-halide monomer, through Suzuki coupling and microwave heating (Fig. 47) [99]. Following similar synthesis methodology, pre-functionalized polymeric aromatic frameworks from mononitrotetrakis(iodophenyl)methane as monomer were prepared, being reduced the pending nitro groups during post-synthesis processes to finally obtain derived PAF-NH_2 solids, which are treated in successive modifications to introduce additional active functions (Fig. 48) [100]. Alternatively, pyrdinium units have also been included as builder fragments in the framework of PAF-50 via condensation of 4-pyridinylboronic acid and cyanuric chloride in toluene, resulting PAFs with cationic centers of quaternary pyridinium ions stabilized into the walls [101]. In this case, it was possible to modify the internal size of the channels through ion-exchange post-synthesis processes. Therefore, after choosing and adjusting the sterically hindered counter ions, the pore diameters were tuned at angstrom scale in the range of 3.4 – 7 Å, being PAF-50 an attractive structure with anion-templated pore apertures with promising applications as polymeric sieve for separation processes (Fig. 49) [102].

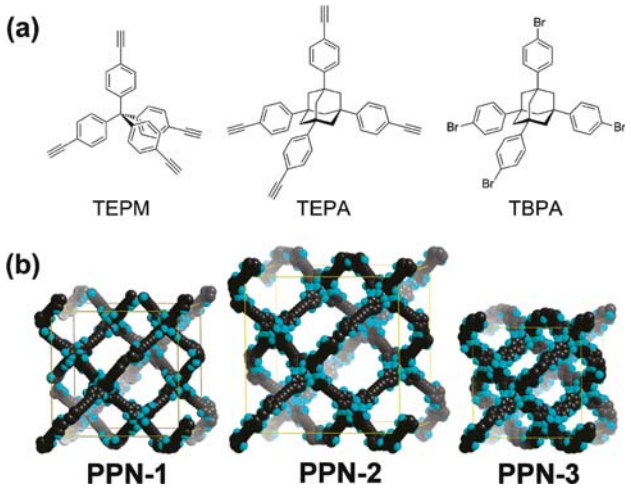

Figure 46. (a) Tetrahedral monomers and (b) the default non-interpenetrated diamondoid networks of the PPNs generated by coupling reactions (TEPM, PPN-1; TEPA, PPN-2; TBPA, PPN-3). Reproduced from [98] with permission from ACS.

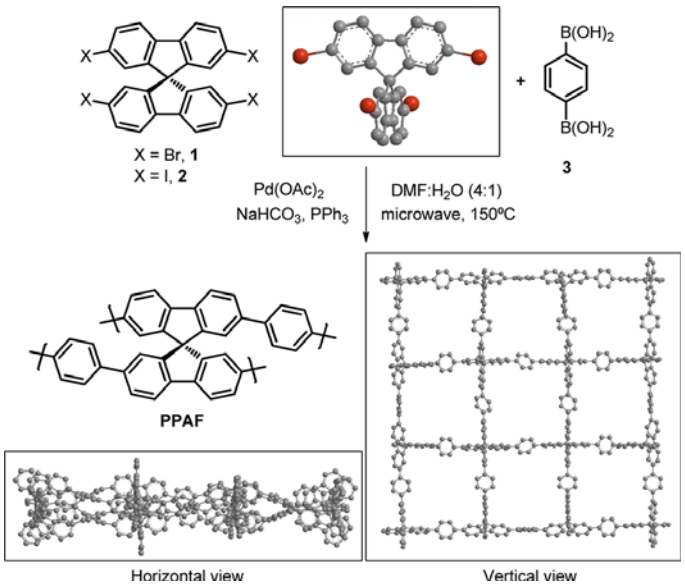

Figure 47. Synthesis of PAF materials based on spirofluorene builders with idealized structures. Reproduced from [99] with permission from ACS.

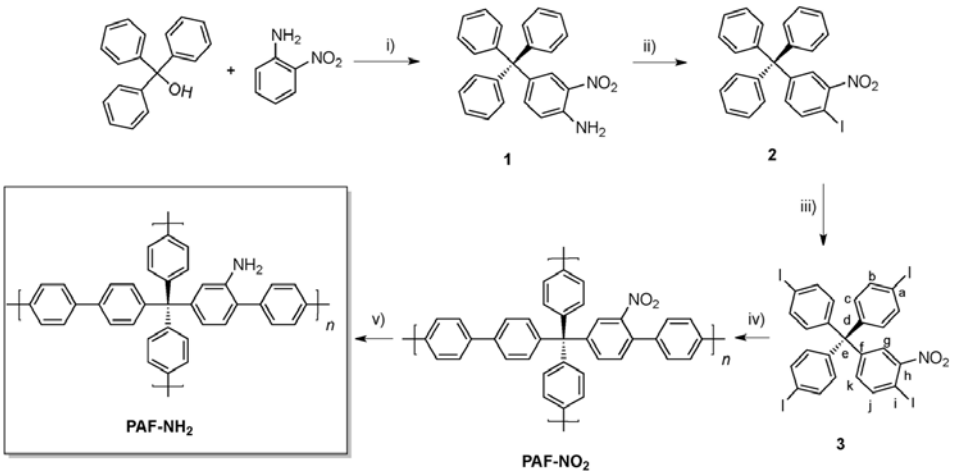

Figure 48. Synthesis of nitro-monomer **3** and functionalized PAFs: PAF-NO_2 and PAF-NH_2. Reagents and conditions: i) HCl, AcOH; ii) $NaNO_2$/KI; iii) I_2, $PhI(OCOCF_3)_2$; iv) 1,4-phenylenediboronic acid, microwave heating, 12 bar, 145 ºC, 10 min; v) $SnCl_2{\cdot}2H_2O$, THF, 90ºC. Reproduced from [100] with permission from Wiley.

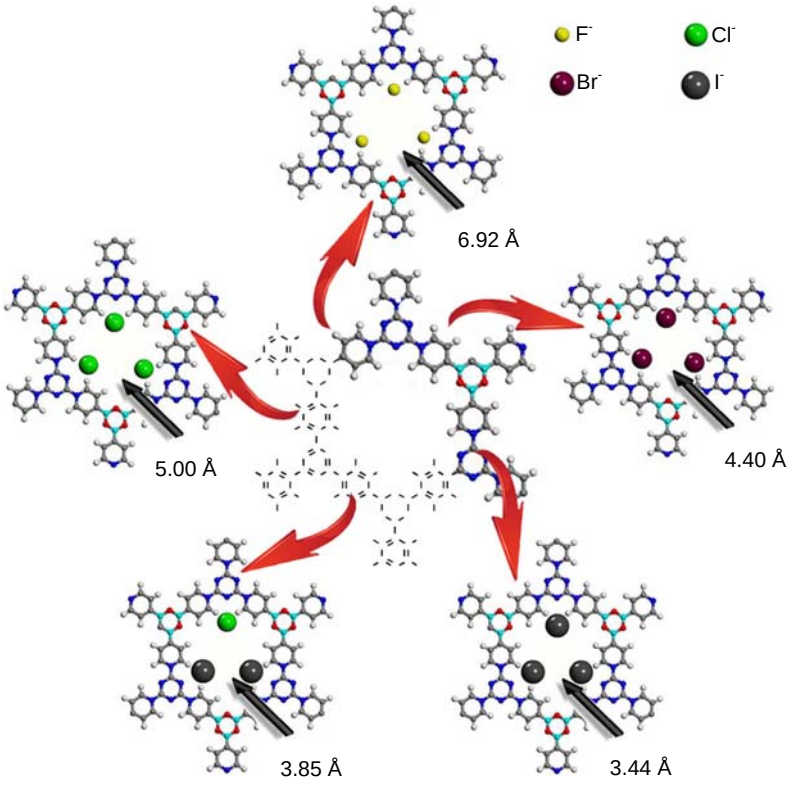

Figure 49. Scheme of preparation of F-PAF-50, Br-PAF-50, 2I-PAF-50 and 3I-PAF-50 from Cl-PAF-50. Reproduced from [102] with permission from McMillan Publishers.

Comparing the different synthesis routes used to obtain open periodic aromatic fameworks, the metal-catalyzed Yamamoto-type Ullmann cross-coupling reaction showed the best condensation results due to the high efficiency to eliminate unreacted termini groups at the monomer building units, favoring the formation of highly connected porous PAFs. So, following this more habitual synthesis pathway novel nitrogen-rich *p*-phenylenediamine and triphenylamine microporous organic polymer based PAFs networks were prepared, exhibiting surfaces area around 2000 m^2g^{-1} and high thermal stability under polar, non-polar or acidic media (Fig. 50) [103,104]. However, currently and as alternative to Yamamoto coupling reaction that need noble metals as catalysts, the Scholl coupling process has been used as low-cost and direct synthetic route to obtain novel PAFs. Specifically, the coupling reaction was catalyzed by $AlCl_3$ occurring between phenyl rings of aromatic monomers, such as triphenylamine, tetraphenylmethane, tetraphenylsilane or tetraphenylgermane, to synthesize novel PAFs families with moderate surface areas (500-1000 m^2g^{-1}) (Fig. 51) [105]. Additionally, Sonogashira-Hagihara coupling reaction was also effective to synthesize pyrene fluorescent porous PAFs (PAF-19 and PAF-20), which were constructed by a tetra-armed unit 1,3,6,8-tetrabromopyrene (TBrPy) with linkers such as 1,4-diethynylbenzene or 1,3,5-

triethynylbenzene. The BET specific surface areas of PAF-19 and PAF-20 were around of 250 m^2 g^{-1} and 700 m^2 g^{-1}, respectively, and H_2O sorption measurements evidenced that their networks were highly hydrophobic [106]. Interestingly, silicon tetrachloride instead of expensive noble metals as catalysts was also used to obtain hierarchical micro and macroporous organic frameworks by cyclotrimerization of acetyl compounds [107].

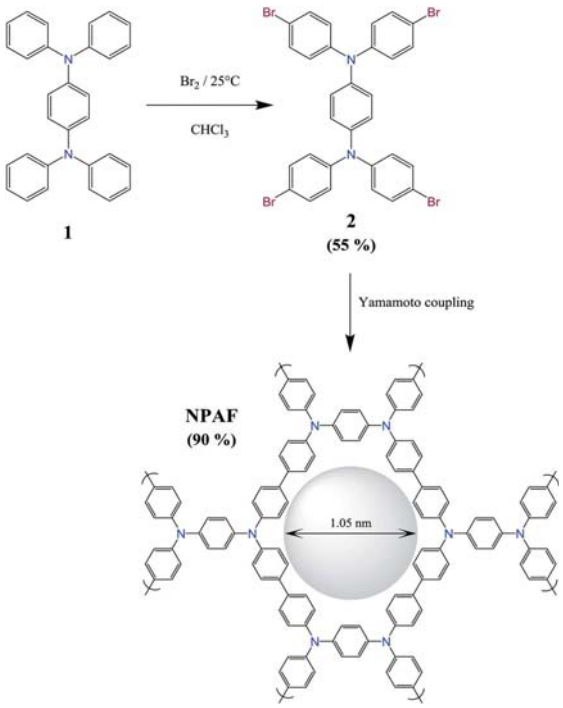

Figure 50. Synthetic route for the preparation of nitrogen-rich based PAFs. Reproduced from [103] with permission from RSC.

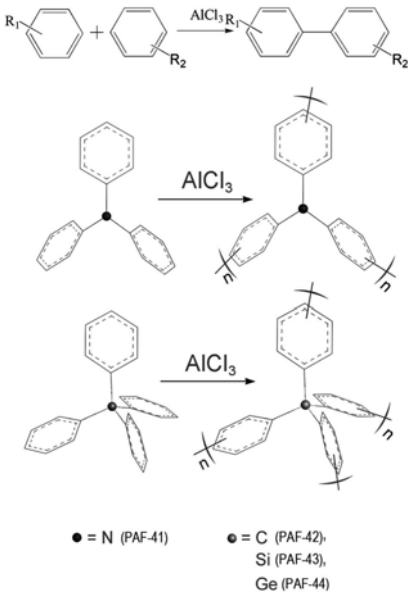

Figure 51. Scholl cross-coupling reaction to obtain extended PAFs-type frameworks. Reproduced from [105] with permission from RSC.

3.1.2. Organosiliceous PAFs

PAF materials can be modified by the inclusion of silisesquioxane units in the structure as covalent attachment point to generate well-defined covalently-linked microporous organic-inorganic hybrid materials by a Yamamoto-type Ullmann cross-coupling reaction. Specifically, JUC-Z1 was prepared from the nanobuilding block *p*-iodo-octaphenylsilsesquioxane (I8OPS). In this case, inorganic silsesquioxane cubes were linearly covalently-linked by biphenyls, offering a highly cross-coupling network and showing spherical morphology with regular micropores. Textural properties analysis evidenced that the hybrid framework had a narrow pore size distribution from 11.8 to 20.0 Å, with a BET surface area around of 300 m^2g^{-1}, being stable up to 400ºC in air (Fig. 52) [108]. So, the presence of organosilicon units into the framework opens the possibilities to incorporate additional functions to PAF materials.

In Table 2, specific surface area and pore size distribution of some PAF materials are summarized to better establish a suitable comparison about their textural properties. Compared with COFs, PAFs exhibit, in general, lower specific surface areas and pore sizes due to their intrinsic irregular internal structure.

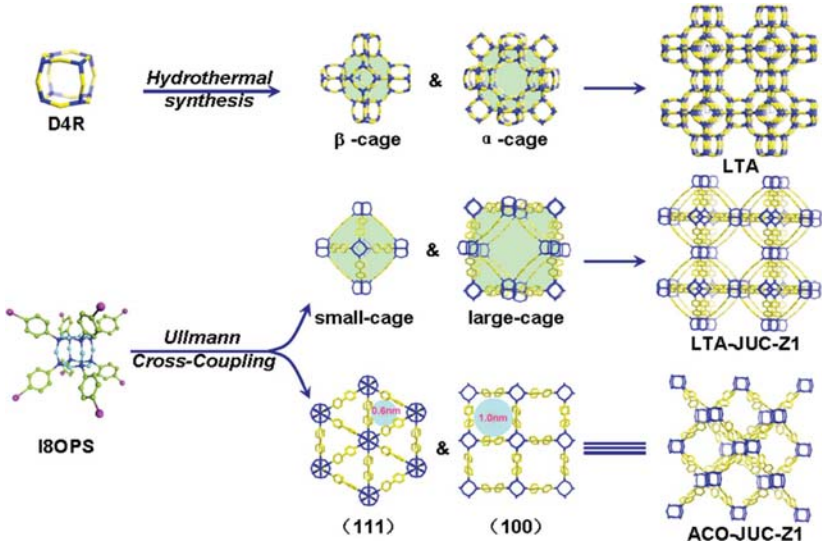

Figure 52. Synthesis route of covalently-linked microporous organic-inorganic hybrid framework JUC-Z1 from I8OPS through Ullmann cross-coupling reaction with an LTA or ACO topology (Si is illustrated in blue and O in yellow for D4R, and Si is illustrated in blue, O in cyan, C in green and I in purple for I8OPS). Reproduced from [108] with permission from RSC.

Table 2.
Textural properties of relevant PAF materials.

PAF-type	BET Surface Area (m^2g^{-1})	Pore Size (Å)	Ref.
PAF-1	5600	15	[94]
PAF-11	700	5-15	[95]
PAF-2	900	11	[96]
PAF-50	100-600	4-7	[102]
Nitrogen-rich based PAFs	2000	10	[103]
PAF-19	250	13	[106]
PAF-20	700	14	
JUC-Z1	300	12-20	[108]

3.2. PAFs: Adsorption, storage and gas uptake applications

All porous aromatic frameworks (PAFs) with diamond-like structure exhibit not only an exceptional high stability and regularity, but also significant surface areas and associated porosity. These characteristics together with their hydrophobic – hydrophilic properties, based on the nature of the aromatic organic builders included in the network, are driving forces to study adsorption and storage capacities. In fact, from multi-scale simulation approaches, the structures of PAFs (so-called PAF-30X, X=1-4, where 3 means 3D structure and X denotes the number of structural phenyl rings), which were prepared by replacing the C-C bond in diamond structure with single or multiple phenyl rings, were used as models to evaluate their hydrogen storage performance. The results revealed that the hydrogen uptakes of PAFs are influenced by their molecular density and free porous volume. Among the four considered structures, PAF-304 and PAF-303 showed higher hydrogen uptake capacity than, even, recently described COFs (such as the COF-102), and at 298 K and 100 bar, COF-304 presents a gravimetric hydrogen uptake of ~7.0 wt.%, which was the highest among all of the studied PAFs (Fig. 53) [109, 110]. Furthermore, the presence of lithium atoms or, even, lithium tetrazolide moieties into the porous aromatic frameworks (PAF-1 and PAF-4) increases the hydrogen storage capacity due to the elevated number of binding sites with low interaction energies for hydrogen due to the presence of lithium-based units (Fig. 54) [111, 112].

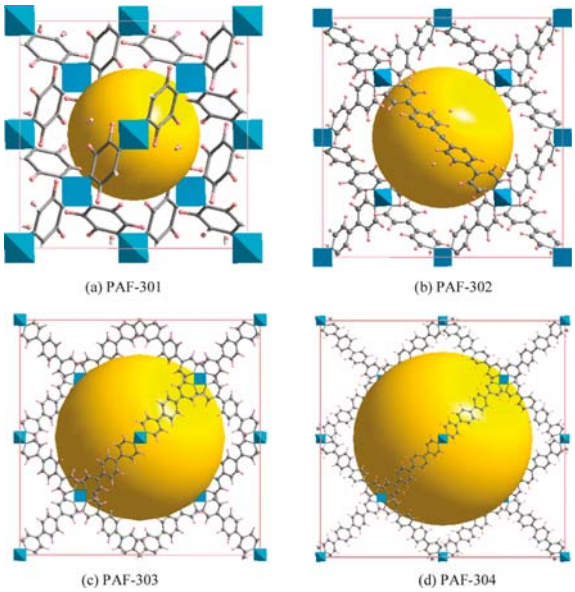

Figure 53. Optimized morphology and geometry of different PAFs: (a) PAF-301, (b) PAF-302, (c) PAF-303, and (d) PAF-304. Carbon: gray; hydrogen: pink; carbon tetrahedral polyhedron: blue; pores in 3D PAFs: yellow. Reproduced from [109] with permission from ACS.

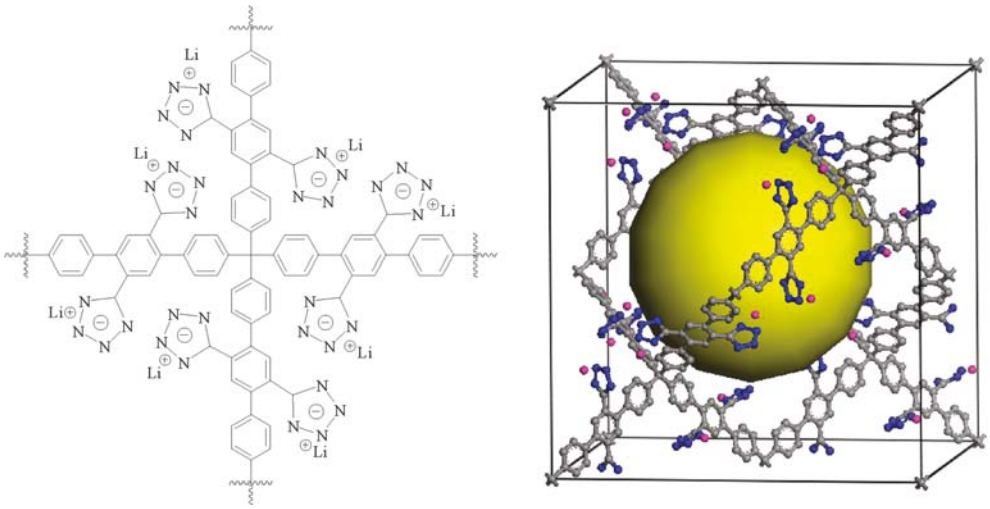

Figure 54. The building block (left) and unit cell (right) of the proposed porous aromatic framework (PAF-4) containing Li(+)-CHN_4(-) (lithium tetrazolide) moieties. The yellow ball corresponds to the free volume. Reproduced from [111] with permission from ACS.

Interesting results have also been obtained associated to the confinement of ammonia borane molecules (AB) into the free volume of PAF-1 structure [113]. AB is considered a potential candidate for on-board hydrogen storage owing to its high stoichiometric hydrogen content (19.6 wt.%) and moderate dehydrogenation temperature. However, its slow dehydrogenation kinetics, below 100ºC, and easy release of volatile by-products (ammonia, borazine, and diborane), can limit its application. Therefore, the use of porous aromatic frameworks such as PAFs with low density, high accessibility and stability as containers is an interesting option to confine AB molecules. Specifically, AB can be fully confined within the

nanopores when the weight ratio of AB/PAF-1 is around 1:1, starting to dehydrogenate at very low temperatures (~50°C) in absence of any volatile by-products. Moreover, ~4 wt.% of hydrogen was generated in the first 25 min at 75°C which is 27 times higher than the pristine AB, exhibiting higher production kinetics at low temperatures (Fig. 55).

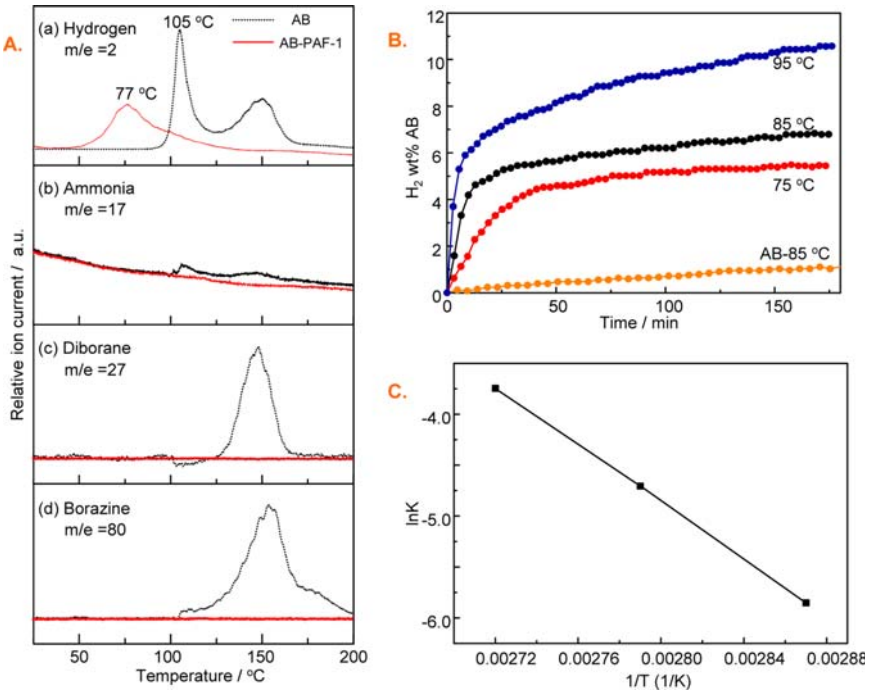

Figure 55. (a) TPD-MS spectra of AB (black ash line) and AB-PAF-1 (red line). (b) Time dependences of hydrogen release from AB-PAF-1 at 95 °C (blue), 85 °C (black), 75 °C (red), and pristine AB at 85 °C (orange). (c) Arrhenius treatment of PCT rate data yields a straight line with a gradient that is proportional to the activation energy of AB-PAF-1 ($E_a \approx 116$ kJ mol^{-1}). Reproduced from [113] with permission from ACS.

Molecular simulation studies, using grand-canonical Monte Carlo, were also applied to PAFs structures by introducing polar organic groups to biphenyl builder units with the objective to investigate their adsorption and separating ability toward methane, CO_2 and other noble gases such as Xenon, thanks to the strong interaction established between adsorbed molecules and organic linkers [114, 115]. Between the simulated functional PAFs-type materials, it was found that tetrahydrofuran-like ether-functionalized PAF-1 exhibited higher adsorption capacity for CO_2 at 1 bar and 298 K (10 mol per kg of adsorbent) and also higher selectivities for CO_2/CH_4, CO_2/N_2, CH_4/H_2 and CO_2/H_2 mixtures when compared with the single amine functionality. The electrostatic interactions were identified as a decisive factor to explain the high CO_2 selectivities of functional PAFs, showing that post-functionalization of PAFs materials with tetrahydrofuran-like ether groups or, even, with other nitrogen-containing units (such as imidazole, pyridine or aminoethane) is a promising route to increase CO_2 adsorption capacity and selectivity at ambient pressures [116, 117, 118].

Following this line, phthalimidomethyl-functionalized versions of PAF-1-type materials showed experimentally high CO_2 adsorption capacities (~100 cm^3g^{-1} of CO_2 uptake) [119]. Furthermore, these promising theoretical gas uptake properties were also confirmed for different PAFs, obtained through Yamamoto-type Ullmann reactions, containing quadricovalent silicon (PAF-3) and germanium (PAF-4) units. In these cases, low pressure gas uptake tests showed that PAF-3 exhibited the highest heat of adsorption (Qst) of hydrogen (6.6 kJ mol^{-1}) and carbon dioxide (19.2 kJ mol^{-1}), while PAF-4 had the highest Qst for methane adsorption (23.2 kJ mol^{-1}), among PAFs-type materials. Moreover, gas molecular recognition at 273 K was carried out, resulting that only environmental friendly gases, such as carbon dioxide and methane, were adsorbed onto this family of porous aromatic structures (Fig. 56) [120, 121]. Impregnation of porous organic structures, such as PAF-5, with branched polyethylenimine (~40%wt) was also useful to generate stable materials with high capacity and selectivity of CO_2 capture at 313 K (11.1 wt% under 0.15 atm of CO_2), showing fast adsorption/desorption kinetics (within 10 min) and low energy interaction for regeneration of the adsorbents (413 K under 1 atm CO_2 for 11.1 wt% working capacity) (Fig. 57) [122]. In this line, non-interpenetrated diamondoid polymer porous networks (so-called PPN), prepared from similar synthesis routes, exhibited also high CH_4 and CO_2 uptake capacities [123].

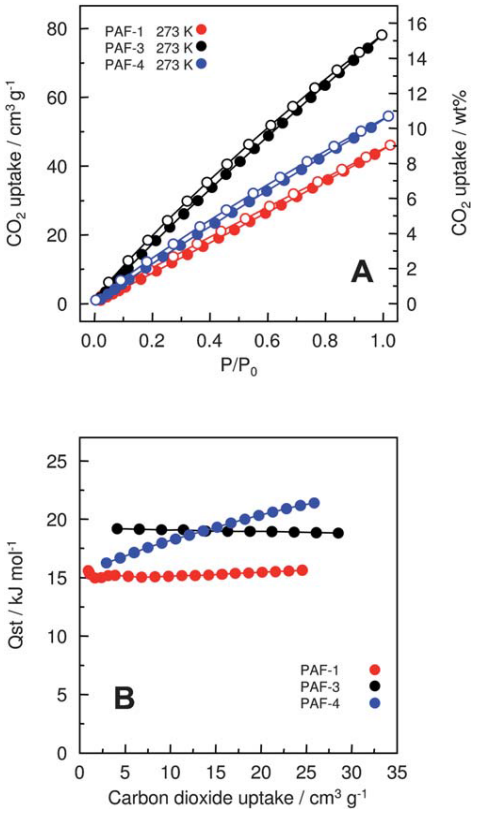

Figure 56. (a) CO_2 isotherms of PAF-1, PAF-3 and PAF-4 at 273 K. Adsorption: solid symbols; desorption: open symbols; (b) CO_2 heat of adsorption (Q_{stCO2}) of PAF-1, PAF-3 and PAF-4 dependent of the adsorbed CO_2. Reproduced from [120] with permission from RSC.

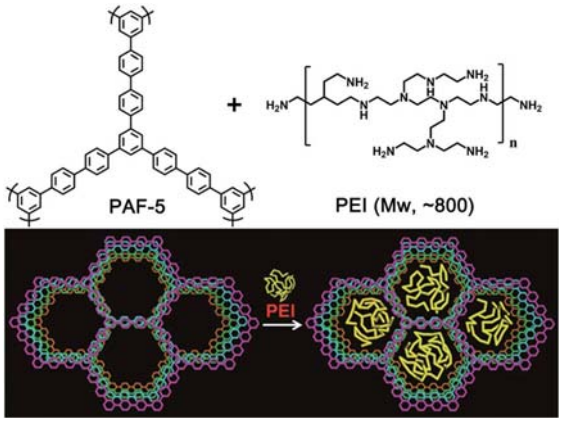

Figure 57. Scheme of PAF-5 impregnated with branched polyethylenimine. Reproduced from [122] with permission from RSC.

The gas storage and adsorption heat (Q_{st}) showed for several carbonized PAF-1-type materials (4.5 mmol g^{-1} CO_2 at 273 K and 1 bar) is highly remarkable. These modified PAFs showed excellent selectivity over other gases, such high as 209 at a 15/85 CO_2/N_2 ratio. In addition, the CO_2/CH_4 adsorption selectivity oscillated around 7.8-9.8 at a 15/85 CO_2/CH_4 ratio at $0 < p < 40$ bar, which is useful for gas separation, being the CO_2/H_2 adsorption selectivity appriximately 392 at 273 K and 1 bar for 20/80 CO_2/H_2 mixtures. These results were analyzed through molecular simulations, showing that the high selectivity exhibited by PAFs materials was related to the difference of isosteric heats (DIH), and was independent of the molar fraction at zero pressure [124]. Furthermore, pre-introduction of extra-carbon source into the PAF-1-type materials, such as furfuryl alcohol, followed by the thermolytic carbonization process and KOH activation were also useful treatments to obtain high CO_2 uptake capacities at low pressures (4.0 mmol g^{-1} at 295 K and 1 bar) (Fig. 58). Thus, these carbonized PAF-1-type materials showed excellent possibilities to be used in capture of CO_2 processes [125, 126, 127].

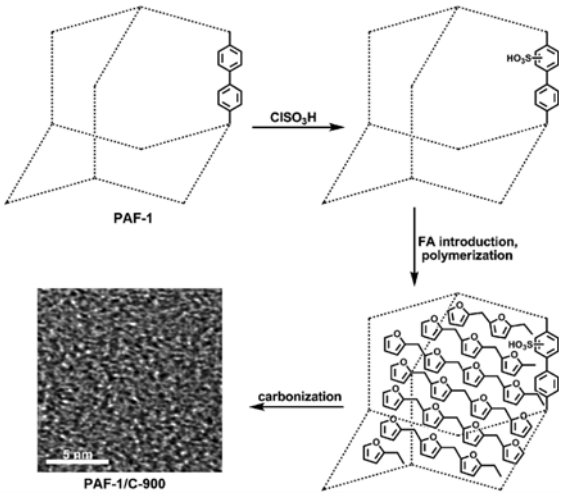

Figure 58. Scheme of the procedures for the preparation of carbonized PAF-1 at 900ºC with the previous introduction of furfuryl alcohol as extra-carbon source. Reproduced from [126] with permission from RSC.

Interestingly, it is possible to take advantage of the π-complexation properties exhibited by the polymeric aromatic frameworks to increase the uptake capacities of the PAFs for different gases separation processes. This phenomenon has been reported for PAF-1 functionalized with Ag(I) ion (PAF-1-SO_3Ag) that showed exceptional high ethylene/ethane adsorption selectivity (S_{ads}: 27 to 125), clearly improving the results obtained with zeolites and MOFs (Fig. 59) [128]. In this case, the formation of π-complexation between ethylene molecules and Ag(I) ions was confirmed by the high isosteric heats of C2H4 adsorption.

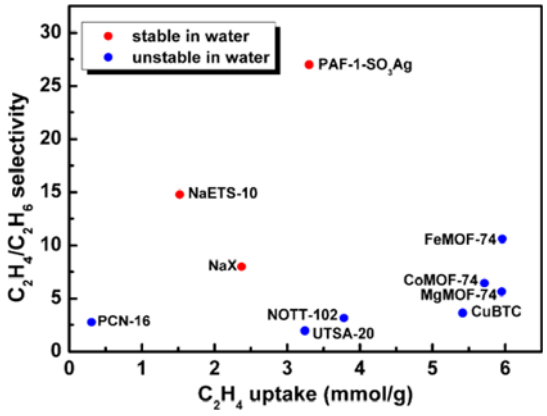

Figure 59. Calculations of C_2H_4/C_2H_6 adsorption selectivity vs gravimetric uptake capacity of ethylene for adsorption from an equimolar C_2H_4/C_2H_6 mixture at 296 K and 100 kPa. Reproduced from [128] with permission from ACS.

Recently, the benefits observed when porous aromatic solids are incorporated in gas-separation polymer membranes with intrinsic microporosity were verified. Normally, porosity

loss, known as physical aging, in glassy polymers strongly reduces their long term use for gas separations processes. This important drawback is avoided with the introduction of PAF-1 together with these polymers because the performances and properties offered by this type of membrane composite implied a substantial improvement in different aspects. Specifically, hydrogen permeability was drastically increased by 375 % to 5500 Barrer, physical aging was better controlled favoring the selectivity for H_2 over N_2 to increase from 4.5 to 13 over 400 days of aging, and the improvement with age of the membrane was exploited to recover up to 98 % of H_2 from gas mixtures with N_2. So, the composite membrane based on polymer side chains attached in PAF-1 free porous volume maintained the H_2 preferential transport pathways [129].

In addition, the high gas uptake capacity exhibited by PAFs-type materials has also been taken as advantage to capture another type of organic pollulant compounds or even iodine vapor that is one of the main components present in waste streams produced for nuclear energy generation. In this case, the iodine vapor uptake of PAF-1 and JUC-Z2 materials were 1.8 and 1.4 $g.g^{-1}$, respectively, at 298 K per 40 Pa, being extremely high for such low pressure sorption conditions. Moreover, these PAFs were capable to adsorb iodine over water with selectivities of 5.1 and 6.5, respectively, showing the potentiality of ordered polymeric structures to obtain nuclear energy trough more efficient, safe and environmental-friendly conditions [130, 131]. On the other hand, the adsorption properties of these porous aromatic frameworks were also useful to storage and progressively release active principles, such as drugs. It is the case of 2-dimensional PAF-6 solid, based on trigonal building units together with piperazine as linear linker, which exhibited interesting drug release ability towards ibuprofen, showing the possibilities of PAFs for biomedical applications [132].

3.3. PAFs: Catalytic applications

3.3.1. One-pot cascade processes

The regular porosity, hydrothermal stability and the possibility to use the rigid planar aromatic builders as authentic platform linkers are key factors to use PAFs materials as multi-functional active catalysts to carry out consecutive or cascade catalytic reactions. In these platform linkers is possible to incorporate different active functions, isolated, stabilized and separated at fixed molecular distances, without blocking internal pore volume. However, up to now, few studies related with the use of ordered polymeric aromatic frameworks as recyclable solid catalysts have been published, being a field in expansion.

It is remarkable the work performed by Merino *et al.* [**99**] based on PAFs constructed by 9,9'-spiro-bisfluorene units which were used as effective support of different active

functions. In detail, the solid was functionalized with acid and base active sites and used as a bi-functional recoverable catalyst in a model one-pot cascade process (hydrolysis of an acetal and a Knoevenagel condensation), avoiding the inconvenience of homogeneous catalysts where acid and base sites are mutually cancelled. Functionalization with acid groups was achieved from the corresponding tetra-iodo spiro-bisfluorene monomer with a simple post-treatment with chlorosulfonic acid (PPAF-SO_3H). Next, base sites were introduced by additional functionalization of sulfonic-PAF with amino groups in two steps. First, nitration with nitric acid generates the nitro-functionalized solid (PAF-SO_3H-NO_2) with NO_2 groups located on non-sulfonated aromatic rings. Second, the nitro groups were reduced, yielding PAF-SO_3H-NH_2 catalyst (Fig. 60). This bi-functional acid-base PAF was capable to perform a cascade reaction that involved two steps: an acid-catalyzed hydrolysis of acetal to produce benzaldehyde intermediate and the subsequent base-catalyzed Knoevenagel reaction to yield 2-benzylidenemalononitrile. The kinetic results showed complete conversion with 100% of selectivity after 1 hour of reaction (Fig. 61), being the acid-base PAF stable and ready for several recycles (up to eight times with only small loss of activity)**.** Physical catalysts mixture formed by independent PPAF-SO_3H + PPAF-NH_2 efficiently catalyzed the same tandem reaction, although lower selectivity was achieved under the same reaction conditions. However, for those reactions in which it was not necessary that the active centers were close, these physical mixtures of PAFs catalysts present advantages versus the bi-functional systems, such as easier preparation and wider possibilities for using catalytic systems with different acid/base ratio and/or different strength [133]. In fact, the exceptional stability of these materials makes them advantageous over comparable metal–organic framework materials (MOFs) [134].

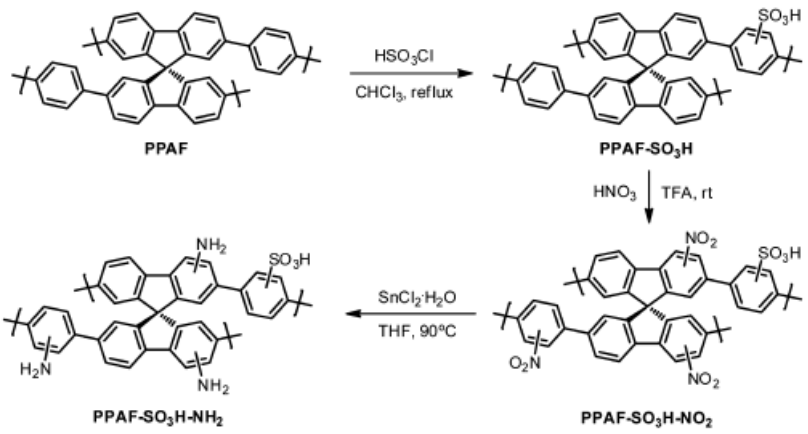

Figure 60. Synthesis of bi-functional PAF-SO_3H-NO_2. Reproduced from [99] with permission from ACS.

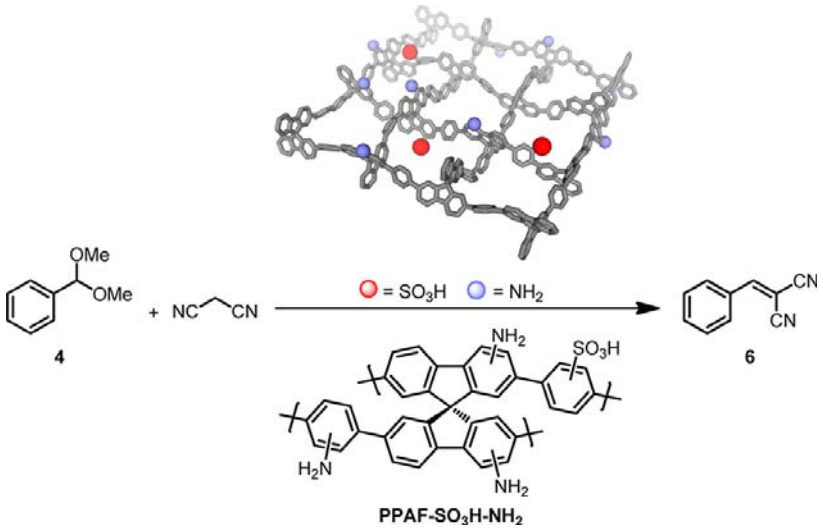

Figure 61. PAF-SO_3H-NH_2 catalyzed one-pot tandem reaction of benzaldehyde dimethylacetal and malononitrile. Reproduced from [99] with permission from ACS.

Similarly, dual functionalization of PAF-1 material was also carried out with the objective to incorporate two opposite sites*, i. e.,* strong acid and strong base centers into the same porous aromatic structure through stepwise post-synthesis modification. The resulting bi-functionalized PAF-1-type solid showed excellent performances for catalytic cascade reactions, exhibiting higher chemical stability than mesoporous silicas and MOFs, which contained similar active sites. More in detail, the two antagonistic functional groups were grafted onto PAF-1 stable support by first nitration and then reduction process to obtain PAF-1-NH_2, which was additionally modified by N-BOC-bromoethylamine to yield PAF-1-$NHCH_2CH_2NHBOC$ with protected pending amino groups. After, sulfonation followed by deprotection allowed obtaining the desired bi-functional catalyst PAF-1-$NHCH_2CH_2NH_2$–SO_3H, being the basic and acidic catalytic sites located and stabilized onto the organic polymeric framework (Fig. 62). This bi-functional PAF-1 material was highly effective catalyzing the one-pot two-step deacetalization–Henry reaction, opening the door for dual functionalization of PAFs as a new platform solids for heterogeneous cascade or consecutive catalysis [135].

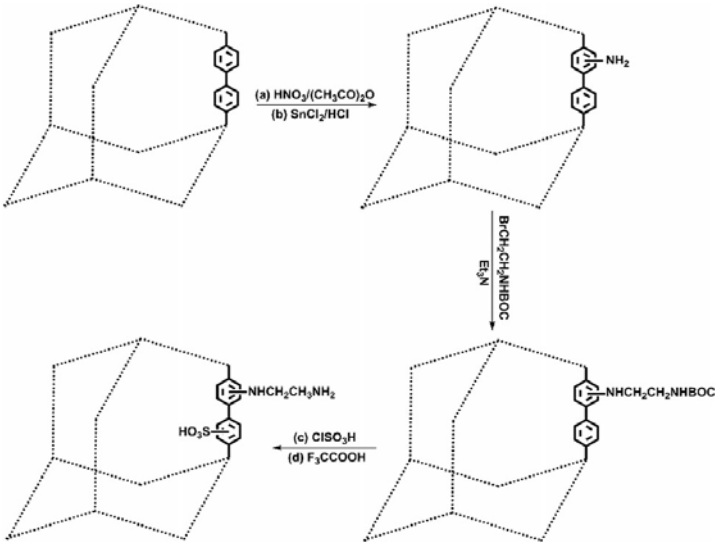

Figure 62. Scheme of stepwise post-synthesis modification of PAF-1 to anchor two opposite functional groups, *i. e.,* strong acid and strong base sites to yield PAF-1-$NHCH_2CH_2NH_2$–SO_3H. Reproduced from [135] with permission from RSC.

3.3.2. Other catalytic reactions: Hydrogenation, Oxidation

As it was commented in the previous synthesis section for PAFs, starting from mononitrotetrakis(iodophenyl)methane as monomer, novel pre-functionalized porous aromatic frameworks were prepared and modified through post-synthesis treatments to be finally used as supports for organometallic catalysts. Specifically, neutral coordinate imino-pyridine Schiff base (PAF-NPy) or chiral bis-amino (PAF-NPro) ligands were obtained by post-synthetic processes of previously formed PAF-NH_2, being modified with copper (I) or rhodium (I) complexes to generate new active supported transition-metal solid catalysts (PAF-NN-M). These solid catalysts showed activity and selectivity similar to homogeneous organocatalysts for promoting several reactions, such as, cyclopropanation, hydrogenation and enenatioselective multi-component reactions to give propargylamines with high efficiency (Fig. 63) [**100**].

On the other hand, although still unexplored, the presence of metallic nanoparticles supported onto porous aromatic PAF-type matrixes would be useful to generate effective highly stable redox solid catalysts, while additional active functions are located onto the organic framework, generating multi-functional recyclable catalysts. Previous studies based on polymeric networks constructed by covalent linked triazine fragments with numerous bi-pyridyl units coordinated with Pt species would support this possibility. These later organic solids were tested for the direct methane oxidation to methanol in concentrated sulfuric acid as oxidant at low reaction temperatures, yielding ca. 250 TONs and indicating the potential of

modified PAFs with additional metal active centers to generate effective oxidation catalysts [136].

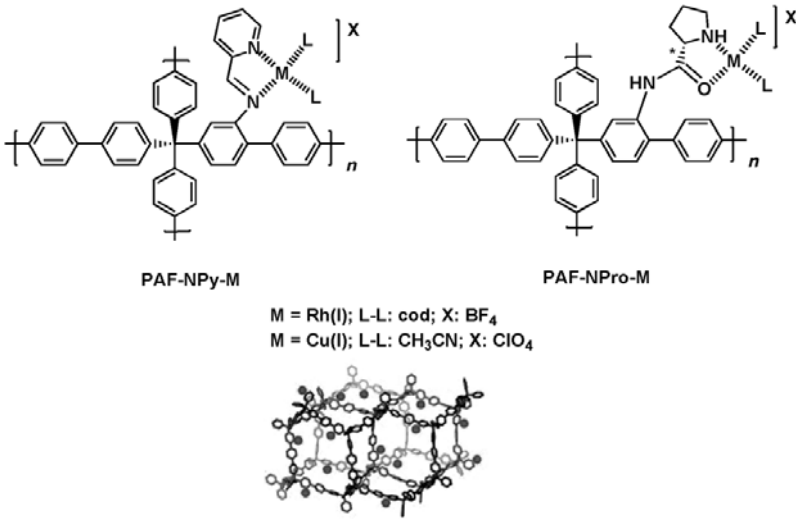

Figure 63. Heterogenized PAF-transition-metal complexes. Reproduced from [100] with permission from Wiley.

3.4. PAFs: Applications for nanotechnology: Sensors and electronic devices

Similarly to conventional COFs, porous aromatic frameworks, PAFs, are constructed from the assembly of rich-electron organic fragments, facilitating the formation of organized sub-domains based on π-conjugated systems. In the case of PAFs-type materials, more robust and stable low-density charged networks are obtained, maintaining high homogenous distribution of builder units around microporous channels, which favor the use of these solids in sensoring, photoluminescence and optoelectronic applications, in general, related with electron donor-acceptor processes. It is the case of PAFs solids based on fluorescent and electron-donating pyrene scaffold building units which facilitated guest-induced emission changes and encapsulation of C_{60} acceptor molecules, showing promising applications as sensoring materials (Fig. 64) [137]. Alternatively, the presence of fluorescence quencher organic moieties, electronically interacting with the π-conjugated 2D structure of PAF-6-type materials, was decisive for the detection of nucleic acid and nuclease activity by simply mixing dye-labeled single-stranded DNA probes with PAF materials. The detected sensibility for this system would suggest that PAFs can be used as excellent sensing platform for bioanalysis and biomedicine [138].

Another sensoring possibility is the incorporation of aromatic halide guests onto the framework of PAFs materials based on the assembly of phosphorescent chromophore builders, such as naphthalenediimide units. It is remarkable as the phosphorescent efficiency of these solids is strongly increased owing to the structural interaction between aromatic halide

compounds and polymeric organic networks through favorable charge-transfer phenomenon, facilitating an over population of the triplet state. The long lifetime of these photo-induced states confirms the potentiality of these phosphorescent porous organic solids as effective oxygen generators or with application for bio-imaging [139].

Two-dimensional JUC-Z2 PAF-type material, formed by stacked polymer sheets with an *hcb* topology, was described as an effective electroactive organic molecular sieve. Specifically, after doping of the polytriphenylamine network with I_2, JUC-Z2 showed typical *para*-type semiconductive properties, being the first example of an electroactive organic framework that exhibited abilities for electrochemistry ion recognition, due to the synergistic favorable combination between uniform micropores and N-atom redox sites (Fig. 65) [140].

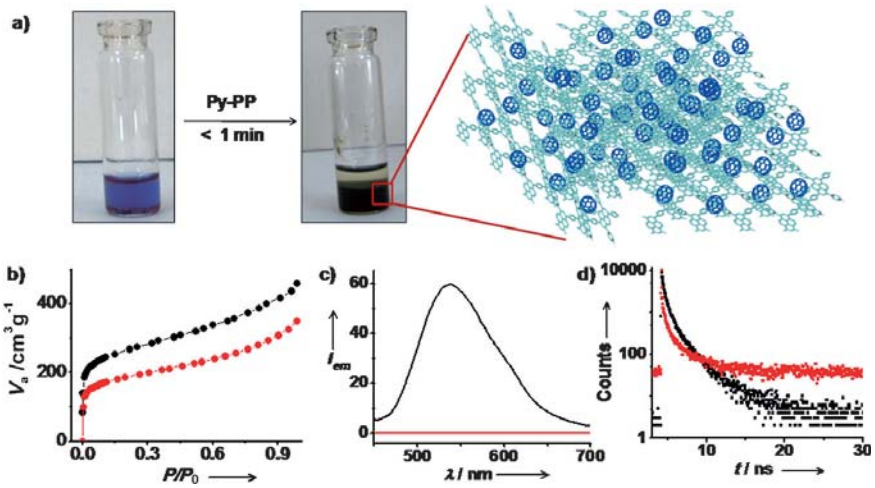

Figure 64. Bucky-ball soaking of Py-PP. (a) Photographs of a saturated solution of C_{60} in toluene (2 mgmL^{-1}) before and after treatment with Py-PP and scheme of C_{60}-loaded Py-PP. (b) N_2 adsorption isotherms (77 K). (c) Solid-state emission spectra and (d) picosecond lifetime decay profiles of Py-PP with (red) and without C_{60} (black). Reproduced from [137] with permission from Wiley.

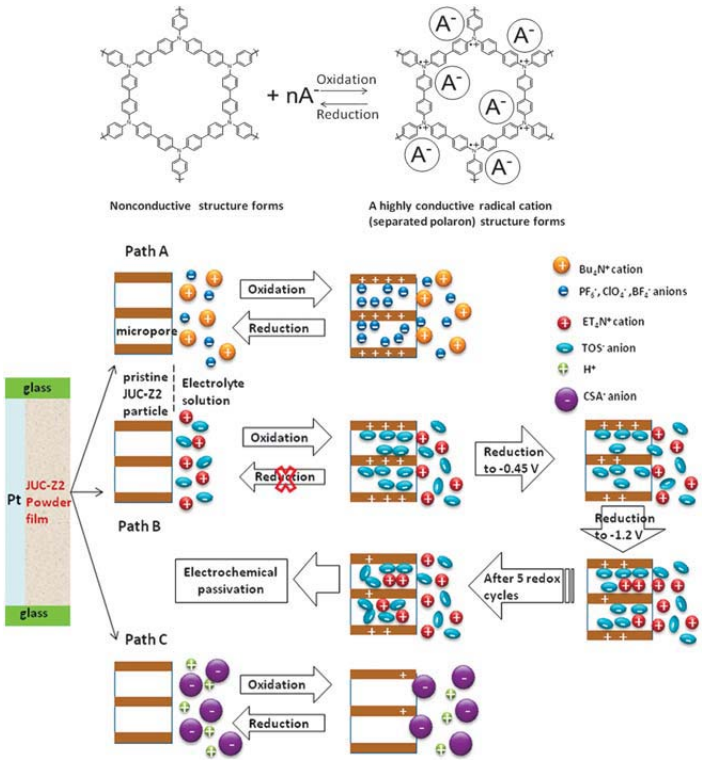

Figure 65. Scheme of electrochemical redox behavior of pristine JUC-Z2 and associated redox processes occurring in either Bu_4NPF_6 (Bu_4NClO_4, Bu_4NBF_4), ET_4TOS or HCSA supporting electrolyte solutions. Reproduced from [140] with permission from RSC.

Recently, promising super-capacitor materials based on PAF-1 materials were also prepared through suitable carbonization processes. The capacitance of the porous carbons, generated by this methodology, was measured both in aqueous and in organic electrolytes. The results showed that those obtained by KOH activation showed high microporous volume combined with mesoporous contribution, which was suitable for charge storage, favoring the fast ion diffusion in the pores, *i. e.,* desired properties for super-capacitors applications. Moreover, it was corroborated that the distribution of the electrolytes in the pores of carbonized PAF-1 solids significantly influenced the capacitance of these porous carbonaceous materials (Fig. 66) [141].

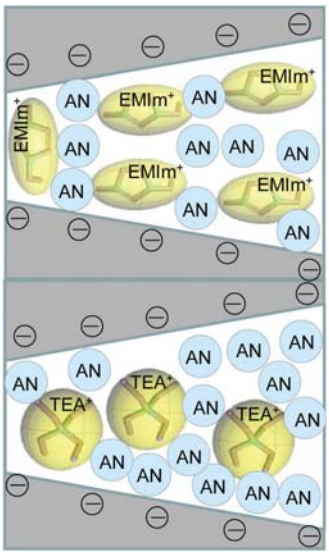

Figure 66. Scheme of packing density of 1-ethyl-3-methylimidazolium ($EMIm^+$) and tetraethylammonium (TEA^+) in the pores of K-PAF-1 (AN: acetonitrile). Reproduced from [141] with permission from RSC.

4. Summary and perspective

Covalent organic frameworks (COFs) and, in particular, their sub-group based on porous aromatic structures (PAFs) are an interesting and emergent materials family with large possibilities in different application fields, such as those more conventional for porous materials (adsorption, separation or catalysis) and those related with sensoring, photoluminescence and optoelectronic, where advanced electron donor-acceptor structures are necessary.

In the case of COFs and PAFs materials, all suitable morphological characteristics and physico-chemical properties to carry out a variety of applications are present: homogeneous porous distribution, high hydrothermal stability and robustness, peculiar hydrophobic-hydrophilic nature, structural regularity, and capability to incorporate different active functions in the planar organic builders (isolated and separated at fixed molecular distances) which convert to these solids as ideal platforms to be used for selective gases separation or adsorption, as effective carriers or as efficient multi-functional catalysts for cascade or consecutive processes. Moreover, π-conjugated array systems, highly charged low-density networks, together with suitable capability to be organically modified with dopants to increase their conductivity or photosensibility, transform COFs or PAFs in authentic nanotechnological advanced materials whose role in the near future probably will be decisive in the design and assembly of versatile photoelectronic devices.

As new synthesis approaches, the use of soft solution processes for the generation of further covalent extended π-conjugated polymeric porous structures in low-dimensions would

be important. In this case, thermodynamic control over equilibrium polymerization is strongly favored by the spontaneous assembly of organic builder units in ordered porous frameworks. These synthesis mechanisms would avoid the use of more demanding and severe conditions (high pressures and temperatures in solvothermal processes), favoring friendly soft preparation routes [142].

Additionally, the possibility to incorporate other organic fragments to generate novel families of COFs or PAFs with, up to now, unknown unique properties would be highly recommendable. In this line, formation of 1D, 2D or 3D organic structured materials by the auto-assembly of photoreactive and nitrogen rich builders, such as rotaxanes or carbazol units, would favor the preparation of novel advanced materials with high gas-uptake capacities or particular senso-electronic properties [143,144].

Furthermore, covalent organic frameworks offer the possibility, practically exclusive into the materials field, to combine catalytic or photocatalytic reactions together with nanotechnological processes (electronic, optical), using only one recyclable material (COFs or PAFs-type) which would act as truthful catalyst-electron donor-acceptor system capable to carry out, in one-pot, multi-step chemical reactive processes.

Acknowledgements

This work was funded by the Spanish Government (Consolider Ingenio 2010-MULTICAT (CSD2009-00050) and MAT2014-52085-C2-1-P) and by the Generalitat Valenciana (Prometeo). The Severo Ochoa program (SEV-2012-0267) is thankfully acknowledged.

References

[1] U. Díaz, D. Brunel, A, Corma, Chem. Soc. Rev. 42 (2013) 4083-4097.

[2] C. Sánchez, B. Julián, P. Belleville, M. Popall, J. Mater. Chem. 15 (2005) 3559-3592.

[3] A.Corma, Cat. Rev. 46 (2004) 369-417.

[4] G. Férey, Chem. Soc. Rev. 37 (2008) 191-214.

[5] C. Sánchez, F. Ribot, New J. Chem. 18 (1994) 1007-1047.

[6] A.P. Wight, M.E. Davis, Chem. Rev. 102 (2002) 3589-3614.

[7] D.A. Loy, J. Shea, Chem. Rev. 95 (1995) 1431-1442.

[8] U. Díaz, A. Vidal-Moya, A. Corma, Microp. Mesop. Mater. 93 (2006) 180-189.

[9] F. Hoffmann, M. Cornelius, J. Morell, M. Fröba, Angew. Chem . Int. Ed. 45 (2006) 3216-3251 and references therein.

[10] S. Inagaki, S. Guan, Y. Fukushima, T. Ohsuna, O. Terasaki, J. Am. Chem. Soc. 121 (1999) 9611-9614.

[11] J.L.C. Rowsell, O.M. Yaghi, Microp. Mesop. Mater. 73 (2004) 3-14.

[12] J. Gascón, A. Corma, F. Kapteijn, F.X. Llabrés i Xamena, ACS Catal. 4 (2014) 361-378.

[13] (a) J. Jiang, F. Su, A. Trewin, C.D. Wood, N.L. Campbell, H. Niu, C. Dickinson, A.Y. Ganin, M.J. Rosseinsky, Y.Z. Khimyak, A.I. Cooper, Angew. Chem. Int. Ed. 46 (2007) 8574-8578;

(b) X. Feng, X. Ding, D. Jiang, Chem. Soc. Rev. 41 (2012) 6010-6022;

(c) S.Y. Ding, W. Wang, Chem. Soc. Rev. 42 (2013) 548-568.

[14] (a) T. Ben, S. Qiu, CrystEngComm 15 (2013) 17-26;

(b) D. Beaudoin, T. Maris, D. Wuest, Nature Chem. 5 (2013) 830-834.

[15] (a) N.B. McKeown, S. Makhseed, P.M. Budd, Chem. Commun. 23 (2002) 2780-2781;

(b) N.B. McKeown, P.M. Budd, K.J. Msayib, B.S. Ghanem, H.J. Kingston, C.E. Tattershall, S. Makhseed, K.J. Reynolds, D. Fritsch, Chem. –Eur. J. 11 (2005) 2610-2620.

[16] (a) J.X. Jiang, A. Trewin, F. Su, C.D. Wood, H. Niu, J.T.A. Jones, Y.Z. Khimyak, A.I. Cooper, Macromolecules 42 (2009) 2658-2666;

(b) C.D. Wood, B. Tan, A. Trewin, H. Niu, D. Bradshaw, M.J. Rosseinsky, Y.Z. Khimyak, N.L. Campbell, R. Kirk, E. Stöckel, A.I. Cooper, Chem. Mater. 19 (2007) 2034-2048;

(c) Y. Xu, S. Jin, H. Xu, A. Nagai, D. Jiang, Chem. Soc. Rev. 42 (2013) 8012-8031.

[17] (a) D. Wang, T. Zhao, X. Zhu, D. Yan, W. Wang, Chem. Soc. Rev. 44 (2015) 4023-4071;

(b) U.H.F. Bunz, K. Seehafer, F.L. Geyer, M. Bender, I. Braun, E. Smarsly, J. Freudenberg, Macromol. Rapid. Commun. 35 (2014) 1466-1496;

(c) Q. Liu, Z. Tang, M. Wu, Z. Zhou, Polym. Int. 63 (2014) 381-392.

[18] A.P. Côté, A.I. Benin, N.W. Ockwig, M. O'Keeffe, A.J. Matzger, O.M. Yaghi, Science 310 (2005) 1166-1170.

[19] M.A.A. Musa, C.-Y. Yin, R.M. Savory, Mater. Chem. Phys. 123 (2010) 5-8.

[20] S.B. Kalidindi, C. Wiktor, A. Ramakrishnan, J. Wessing, A. Schneemann, G. Van Tendeloo, R.A. Fischer, Chem. Commun. 49 (2013) 463-465.

[21] H.M. El-Kaderi, J.R. Hunt, J.L. Mendoza-Cortés, A.P. Côté, R.E. Taylor, M. O'Keeffe, O.M. Yaghi, Science 316 (2007) 268-272.

[22] R. Schmid, M. Tafipolsky, J. Am. Chem. Soc. 130 (2008) 12600-12601.

[23] L. Zhao, C. Zhong, J. Phys. Chem. C 113 (2009) 16860-16862.

[24] J.R. Hunt, C.J. Doonan, J.D. LeVangie, A.P. Côté, O.M. Yaghi, J. Am. Chem. Soc. 130 (2008) 11872-11873.

[25] E.L. Spitler, M.R. Giovino, S.L. White, W.R. Dichtel, Chem. Sci. 2 (2011) 1588-1593.

[26] J. Zhang, L. Wang, N. Li, J. Liu, W. Zhang, Z. Zhang, N. Zhou, X. Zhu, CrystEngComm 16 (2014) 6547-6551.

[27] F.J. Uribe-Romo, J.R. Hunt, H. Furukawa, C. Kloeck, M. O'Keeffe, O.M. Yaghi, J. Am. Chem. Soc. 131 (2009) 4570-4571.

[28] Y.-B. Zhang, J. Su, H. Furukawa, Y. Yun, F. Gándara, A. Duong, X. Zou, O.M. Yaghi, J. Am. Chem. Soc. 135 (2013) 16336-16339.

[29] S. Dalapati, S. Jin, J. Gao, Y. Xu, A. Nagai, D. Jiang, J. Am. Chem. Soc. 135 (2013) 17310-17313.

[30] M. Dogru, A. Sonnauer, A. Gavryushin, P. Knochel, T. Bein, Chem. Commun. 47 (2011) 1707-1709.

[31] B.J. Smith, W.R. Dichtel, J. Am. Chem. Soc. 136 (2014) 8783-8789.

[32] A.P. Côté, H.M. El-Kaderi, H. Furukawa, J.R. Hunt, O.M. Yaghi, J. Am. Chem. Soc. 129 (2007) 12914-12915.

[33] E.L. Spitler, B.T. Koo, J.L. Novotney, J.W. Colson, F.J. Uribe-Romo, G.D. Gutiérrez, P. Clancy, W.R. Dichtel, J. Am. Chem. Soc. 2011, 133 (2011) 19416-19421.

[34] K.T. Jackson, T.E. Reich, H.M. El-Kaderi, Chem. Commun. 48 (2012) 8823-8825.

[35] Z. Li, X. Feng, Y. Zou, Y. Zhang, H. Xia, X. Liu, Y. Mu, Chem. Commun. 50 (2014) 13825-13828.

[36] F.J. Uribe-Romo, C.J. Doonan, H. Furukawa, K. Oisaki, O.M. Yaghi, J. Am. Chem. Soc. 133 (2011) 11478-11481.

[37] Z. Kahveci, T. Islamoglu, G.A. Shar, R. Ding, H.M. El-Kaderi, CrystEngComm 15 (2013) 1524-1527.

[38] M.G. Rabbani, A.K. Sekizkardes, Z. Kahveci, T.E. Reich, R. Ding, H.M. El-Kaderi, Chem. –Eur. J. 19 (2013) 3324-3328.

[39] X. Feng, L. Chen, Y. Dong, D. Jiang, Chem. Commun. 47 (2011) 1979-1981.

[40] E.L. Spitler, J.W. Colson, F.J. Uribe-Romo, A.R. Woll, M.R. Giovino, A. Saldivar, W.R. Dichtel, Angew. Chem. Int. Ed. 51 (2012) 2623-2627.

[41] X. Ding, L. Chen, Y. Honsho, X. Feng, O. Saengsawang, J. Guo, A. Saeki, S. Seki, S. Irle, S. Nagase, V. Parasuk, D. Jiang, J. Am. Chem. Soc. 133 (2011) 14510-14513.

[42] A. Nagai, X. Chen, X. Feng, X. Ding, Z. Guo, D. Jiang, Angew. Chem. Int. Ed. 52 (2013) 3770-3774.

[43] V.S.P.K. Neti, X. Wu, S. Deng, L. Echegoyen, CrystEngComm 15 (2013) 6892-6895.

[44] V.S.P.K. Neti, X. Wu, M. Hosseini, R.A. Bernal, S. Deng, L. Echegoyen, CrystEngComm 15 (2013) 7157-7160.

[45] T.-Y. Zhou, S.-Q. Xu, Q. Wen, Z.-F. Pang, X. Zhao, J. Am. Chem. Soc. 136 (2014) 15885-15888.

[46] D.N. Bunck, W.R. Dichtel, J. Am. Chem. Soc. 135 (2013) 14952-14955.

[47] (a) M. Sassi, V. Oison, J.M. Debierre, S. Humbel, ChemPhysChem 10 (2009) 2480-2485;

(b) J.W. Colson; W.R. Dichtel, Nature Chem. 5 (2013) 453-465.

[48] R. Gutzler, H. Walch, G. Eder, S. Kloft, W.M. Heckl, M. Lackinger, Chem. Commun. 29 (2009) 4456-4458.

[49] O. Ourdjini, R. Pawlak, M. Abel, S. Clair, L. Chen, N. Bergeon, M. Sassi, V. Oison, J.M. Debierre, R. Coratger, L. Porte, L. Phys. Rev. B 84 (2011) 125421/1-125421/9.

[50] A.C. Marele, R. Mas-Ballesté, L. Terracciano, J. Rodríguez-Fernández, I. Berlanga, S.S. Alexandre, R. Otero, J.M. Gallego, F. Zamora, J.M. Gómez-Rodríguez, Chem. Commun. 48 (2012) 6779-6781.

[51] T. Faury, S. Clair, M. Abel, F. Dumur, D. Gigmes, L. Porte, J. Phys. Chem. C 116 (2012) 4819-4823.

[52] D.D. Medina, J.M. Rotter, Y. Hu, M. Dogru, V. Werner, F. Auras, J.T. Markiewicz, P. Knochel, T. Bein, J. Am. Chem. Soc. 137 (2015) 1016-1019.

[53] W. Huang, Y. Jiang, X. Li, X. Li, J. Wang, Q. Wu, X. Liu, ACS Appl. Mater. Interfaces 5 (2013) 8845-8849.

[54] S.S. Han, H. Furukawa, O.M. Yaghi, W.A. Goddard, J. Am. Chem. Soc. 130 (2008) 11580-11581.

[55] H. Furukawa, O.M. Yaghi, J. Am. Chem. Soc. 131 (2009) 8875-8883.

[56] J.L. Mendoza-Cortés, S.S. Han, H. Furukawa, O.M. Yaghi, W.A. Goddard III, J. Phys. Chem. A 114 (2010) 10824-10833.

[57] J.L. Mendoza-Cortés, W.A. Goddard III, H. Furukawa, O.M. Yaghi, J. Phys. Chem. Lett. 3 (2012) 2671-2675.

[58] E. Klontzas, E. Tylianakis, G. Froudakis, J. Phys. Chem. C 113 (2009) 21253-21257.

[59] P. Srepusharawoot, E. Swatsitang, V. Amornkitbamrung, U. Pinsook, R. Ahuja, Int. J. Hydrogen Energ. 38 (2013) 14276-14280.

[60] L.H. Xie, M.P. Suh, Chem. Eur. J., 19 (2013), 11590-11597.

[61] H. Ma, H. Ren, S. Meng, Z. Yan, H. Zhao, F. Sun, G. Zhu, Chem. Commun. 49 (2013) 9773-9775.

[62] H. Oh, S.B. Kalidindi, Y. Um, S. Bureekaew, R. Schmid, R.A. Fischer, M. Hirscher, Angew. Chem. Int. Ed. 52 (2013) 13219-13222.

[63] C.J. Doonan, D.J. Tranchemontagne, T.G. Glover, J.R. Hunt, O.M. Yaghi, Nature Chem. 2 (2010) 235-238.

[64] S. Lin, C.S. Diercks, Y.B. Zhang, N. Kornienko, E.M. Nichols, Y. Zhao, A.R. Paris, D. Kim, P. Yang, O.M. Yaghi, C.J. Chang, Science 349 (2015) 1208-1213.

[65] S.-Y. Ding, J. Gao, Q. Wang, Y. Zhang, W.-G. Song, C.-Y. Su, W. Wang, J. Am. Chem. Soc. 133 (2011) 19816-19822.

[66] P. Pachfule, M.K. Panda, S. Kandambeth, S.M. Shivaprasad, D. Díaz-Díaz, R. Banerjee, J. Mater. Chem. A 2 (2014) 7944-7952.

[67] P. Pachfule, S. Kandambeth, D. Díaz-Díaz, R. Banerjee, Chem. Commun. 50 (2014) 3169-3172.

[68] W. Zhang, P. Jiang, Y. Wang, J. Zhang, Y. Gao, P. Zhang, RSC Adv. 4 (2014) 51544-51547.

[69] R.W. Tilford, J. Lavigne, J. Polymer Preprints 49 (2008) 308.

[70] D.N. Bunck, W.R. Dichtel, Chem. Commun. 49 (2013) 2457-2459.

[71] H. Xu, J. Gao, D. Jiang, Nature hem. 7 (2015) 905-912.

[72] L. Stegbauer, K. Schwinghammer, B.V. Lotsch, Chem. Sci. 5 (2014) 2789-2793.

[73] J. Thote, H.B. Aiyappa, A. Deshpande, D. Díaz-Díaz, S. Kurungot, R. Banerjee, Chem. Eur. J. 20 (2014) 15961-15965.

[74] S. Wan, F. Gándara, A. Asano, H. Furukawa, A. Saeki, S.K. Dey, L. Liao, M.W. Ambrogio, Y.Y. Botros, X. Duan, S. Seki, J.F. Stoddart, O.M. Yaghi, Chem. Mater. 23 (2011) 4094-4097.

[75] S. Jin, X. Ding, X. Feng, M. Supur, K. Furukawa, S. Takahashi, M. Addicoat, M.E. El-Khouly, T. Nakamura, S. Irle, S. Fukuzumi, A. Nagai, D. Jiang, Angew. Chem. Int. Ed. 52 (2013) 2017-2021.

[76] M. Dogru, M. Handloser, F. Auras, T. Kunz, D. Medina, A. Hartschuh, P. Knochel, T. Bein, Angew. Chem. Int. Ed. 52 (2013) 2920-2924.

[77] B.T. Koo, P. Clancy, Mol. Simulat. 40 (2014) 58-70.

[78] S. Chandra, T. Kundu, S. Kandambeth, R. BabaRao, Y. Marathe, S.M. Kunjir, R. Banerjee, J. Am. Chem. Soc. 136 (2014) 6570-6573.

[79] H. Ding, Y. Li, H. Hu, Y. Sun, J. Wang, C. Wang, C. Wang, G. Zhang, B. Wang, W. Xu, D. Zhang, Chem. Eur. J. 20 (2014) 14614-14618.

[80] S.-L. Cai, Y.-B. Zhang, A.B. Pun, B. He, J. Yang, F.M. Toma, I.D. Sharp, O.M. Yaghi, J. Fan, S.-R. Zheng, W.-G. Zhang, Y. Liu, Chem. Sci. 5 (2014) 4693-4700.

[81] D.D. Medina, V. Werner, F. Auras, R. Tautz, M. Dogru, J. Schuster, S. Linke, M. Döblinger, J. Feldmann, P. Knochel, T. Bein, ACS Nano 8 (2014) 4042-4052.

[82] X. Feng, L. Chen, Y. Honsho, O. Saengsawang, L. Liu, L. Wang, A. Saeki, S. Irle, S. Seki, Y. Dong, D. Jiang, Adv. Mater. 24 (2012) 3026-3031.

[83] M. Calik, F. Auras, L.M. Salonen, K. Bader, I. Grill, M. Handloser, D.D. Medina, M. Dogru, F. Loebermann, D. Trauner, A. Hartschuh, T. Bein, J. Am. Chem. Soc. 136 (2014) 17802-17807.

[84] J.W. Colson, A.R. Woll, A. Mukherjee, M.P. Levendorf, E.L. Spitler, V.B. Shields, M.G. Spencer, J. Park, R. Dichtel, Science 332 (2011) 228-231.

[85] L. Xu, X. Zhou, W.Q. Tian, T. Gao, Y.F. Zhang, S. Lei, Z.F. Liu, Angew. Chem. Int. Ed. 53 (2014) 9564-9568.

[86] J.W. Colson, J.A. Mann, C.R. DeBlase, W.R. Dichtel, J. Polym. Sci. A 53 (2015) 378-384.

[87] R.N. Gunasinghe, D.G. Reuven, K. Suggs, X.-Q. Wang, J. Phys. Chem. Lett. 3 (2012) 3048-3052.

[88] W. Zhang, L.-G. Qiu, Y.-P. Yuan, A.-J. Xie, Y.-H.; Shen, J.-F. Zhu, J. Hazard. Mater. 221-222 (2012) 147-154.

[89] S. Wan, J. Guo, J. Kim, H. Ihee, D. Jiang, Angew. Chem. Int. Ed. 47 (2008) 8826-8830.

[90] S. Wan, J. Guo, J. Kim, H. Ihee, D. Jiang, Angew. Chem. Int. Ed. 48 (2009) 5439-5442.

[91] G.H. Fan, X. Li, J.-Y. Liu, G.-Z. He, Comp. Theor. Chem. 1030 (2014) 17-24.

[92] (a) T. Ben, H. Ren, S. Ma, D. Cao, J. Lan, X. Jing, W. Wang, J. Xu, F. Deng, J.M. Simmons, S. Qiu, G. Zhu, Angew. Chem. Int. Ed. 2009, 48 (2009) 9457-9460;
(b) C. Pei, T. Ben, S. Qiu, Mater. Horiz. 2 (2015) 11-21.
[93] A. Trewin, A.I. Cooper, Angew. Chem. Int. Ed. 49 (2010) 1533-1535.
[94] J.M.H. Thomas, A. Trewin, J. Phys. Chem. C 118 (2014) 19712-19722.
[95] Y. Yuan, F. Sun, H. Ren, X. Jing, W. Wang, H. Ma, H. Zhao, G. Zhu, J. Mater. Chem. 21 (2011) 13498-13502.
[96] H. Ren, T. Ben, E. Wang, X. Jing, M. Xue, B. Liu, Y. Cui, S. Qiu, G. Zhu, Chem. Commun. 46 (2010) 291-293.
[97] W. Wang, H. Ren, F. Sun, K. Cai, H. Ma, J. Du, H. Zhao, G. Zhu, Dalton Trans. 41 (2012) 3933-3936.
[98] W. Lu, D. Yuan, D. Zhao, C.I. Schilling, O. Plietzsch, T. Muller, S. Brase, J. Guenther, J. Blumel, R. Krishna, Z. Li, H.-C. Zhou, Chem. Mater. 22 (2010) 5964-5972.
[99] E. Merino, E. Verde-Sesto, E.M. Maya, M. Iglesias, F. Sánchez, A. Corma, A. Chem. Mater. 25 (2013) 981-988.
[100] E. Verde-Sesto, M. Pintado-Sierra, A. Corma, E.M. Maya, J.G. de la Campa, M. Iglesias, F. Sánchez, Chem. –Eur. J. 20 (2014) 5111-5120.
[101] Y. Yuan, F. Sun, F. Zhang, H. Ren, M. Guo, K. Cai, X. Jing, X. Gao, G. Zhu, Adv. Mater. 25 (2013) 6619-6624.
[102] Y. Yuan, F. Sun, L. Li, P. Cui, G. Zhu, Nature Commun. 5 (2014) 4260-4268.
[103] D.E. Demirocak, M.K. Ram, S.S. Srinivasan, D.Y. Goswami, E.K. Stefanakos, J. Mater. Chem. A 1 (2013) 13800-13806.
[104] X. Yang, S. Yao, M. Yu, J.-X Jiang, Macromol. Rapid. Comm. 35 (2014) 834-839.
[105] L. Li, H. Ren, Y. Yuan, G. Yu, G. Zhu, J. Mater. Chem. A. 2 (2014) 11091-11098.
[106] Z. Yan, H. Ren, H. Ma, R. Yuan, Y. Yuan, X. Zou, F. Sun, G. Zhu, Microp. Mesop. Mater. 173 (2013) 92-98.
[107] M. Rose, N. Klein, I. Senkovska, C. Schrage, P. Wollmann, W. Böhlmann, B. Böhringer, S. Fichtner, S. Kaskel, J. Mater. Chem. 21 (2011) 711-716.
[108] Y. Peng, T. Ben, J. Xu, M. Xue, X. Jing, F. Deng, S. Qiu, G. Zhu, Dalton Trans. 40 (2011) 2720-2724.
[109] J. Lan, D. Cao, W. Wang, T. Ben, G. Zhu, J. Phys. Chem. Lett. 1 (2010) 978-981.
[110] B. Lukose, M. Wahiduzzaman, A. Kuc, T. Heine, J. Phys. Chem. C 116 (2012) 22878-22884.
[111] Y. Sun, T. Ben, L. Wang, S. Qiu, H. Sun, J. Phys. Chem. Lett. 1 (2010) 2753-2756.
[112] K. Konstas, J.W. Taylor, A.W. Thornton, C.M. Doherty, W.X. Lim, T.J. Bastow, D.F. Kennedy, C.D. Wood, B.J. Cox, J.M. Hill, A.J. Hill, M.R. Hill, Angew. Chem. Int. Ed. 51 (2012) 6639-6642.
[113] Y. Peng, T. Ben, Y. Jia, D. Yang, H. Zhao, S. Qiu, X. Yao, J. Phys. Chem. C 116 (2012) 25694-25700.
[114] Q. Wang, H. Wang, S. Peng, X. Peng, D. Cao, J. Phys. Chem. C 118 (2014) 10221-10229.
[115] M. Errahali, G. Gatti, L. Tei, L. Canti, A. Fraccarollo, M. Cossi, L. Marchese, J. Phys. Chem. C 118 (2014) 10053-10060.

[116] R. Babarao, S. Dai, D. Jiang, Langmuir 27 (2011) 3451-3460.

[117] J. Fu, J. Wu, R. Custelcean, D. Jiang, J. Colloid Interface Sci. 438 (2015) 191-195.

[118] A. Fraccarollo, L. Canti, L. Marchese, M. Cossi, Langmuir 30 (2014) 4147-4156.

[119] S.J. Garibay, M.H. Weston, J.E. Mondloch, Y.J. Colón, O.K. Farha, J.T. Hupp, S.T. Nguyen, CrystEngComm 15 (2013) 1515-1519.

[120] T. Ben, C. Pei, D. Zhang, J. Xu, F. Deng, X. Jing, S. Qiu, Energy Environ. Sci. 4 (2011) 3991-3999.

[121] C. Pei, T. Ben, Y. Cui, S. Qiu, Adsorption 18 (2012) 375-380.

[122] S. Sung, M.P. Suh, J. Mater. Chem. A 2 (2014) 13245-13249.

[123] D. Yuan, W. Lu, D. Zhao, H.-C. Zhou, Adv. Mater. 23 (2011) 3723-3725.

[124] Z. Yang, X. Peng, D. Cao, J. Phys. Chem. C 117 (2013) 8353-8364.

[125] T. Ben, Y. Li, L. Zhu, D. Zhang, D. Cao, Z. Xiang, X. Yao, S. Qiu, Energy Environ. Sci. 5 (2012) 8370-8376.

[126] Y. Zhang, B. Li, K. Williams, W.-Y. Gao, S. Ma, Chem. Commun. 49 (2013) 10269-10271.

[127] Y. Li, T. Ben, B. Zhang, Y. Fu, S. Qiu, Sci. Rep. (2013) 32420.

[128] B. Li, Y. Zhang, R. Krishna, K. Yao, Y. Han, Z. Wu, D. Ma, Z. Shi, T. Pham, B. Space, J. Liu, P.K. Thallapally, J. Liu, M. Chrzanowski, S. Ma, J. Am. Chem. Soc. 136 (2014) 8654-8660.

[129] C.H. Lau, K. Konstas, A.W. Thornton, A.C.Y. Liu, S. Mudie, D.F. Kennedy, S.C. Howard, A.J. Hill, M.R. Hill, Angew. Chem. Int. Ed. 54 (2015) 2669-2673.

[130] C. Pei, T. Ben, S. Xu, S. Qiu, J. Mater. Chem. A 2 (2014) 7179-7187.

[131] H. Ren, T. Ben, F. Sun, M. Guo, X. Jing, H. Ma, K. Cai, S. Qiu, G. Zhu, J. Mater. Chem. 21 (2011) 10348-10353.

[132] H. Zhao, Z. Jin, H. Su, X. Jing, F. Sun, G. Zhu, Chem. Commun. 2011, 47 (2011) 6389-6391.

[133] S. Xu, S. Roy, T. Ben, C. Pei, S. Qiu, J. Mater. Chem. A 3 (2015) 2628-2633.

[134] E. Merino, E. Verde-Sesto, E.M. Maya, A. Corma, M. Iglesias, F. Sánchez, Appl. Catal. A: Gen. 469 (2014) 206-212.

[135] Y. Zhang, B. Li, S. Ma, Chem. Commun. 50 (2014) 8507-8510.

[136] R. Palkovits, M. Antonietti, P. Kuhn, A. Thomas, F. Schüth, Angew. Chem.Int. Ed. 48 (2009) 6909-6912.

[137] K.V. Rao, S. Mohapatra, T.K. Maji, S.J. George, Chem. –Eur. J. 18 (2012) 4505-4509.

[138] C. Song, G.-Y. Wang, H.-Z. Wang, Y.-J. Wang, D.M. Kong, J. Mater. Chem. B 2 (2014) 1549-1556.

[139] V. Martínez-Martínez, R. Sola-Llano, S. Furukawa, Y. Takashima, I. López-Arbeloa, S. Kitagawa, ChemPhysChem 15 (2014) 2517-2521.

[140] T. Ben, K. Shi, Y. Cui, C. Pei, Y. Zuo, H. Guo, D. Zhang, J. Xu, F. Deng, Z. Tian, S. Qiu, J. Mater. Chem. 21 (2011) 18208-18214.

[141] Y. Li, S. Roy, T. Ben, S. Xu, S. Qiu, Phys. Chem. Chem. Phys. 16 (2014) 12909-12917.

[142] R. Tanoue, R. Higuchi, N. Enoki, Y. Miyasato, S. Uemura, N. Kimizuka, A.Z. Stieg, J.K. Gimzewski, M. Kunitake, ACS Nano 5 (2011) 3923-3929.

[143] I.-H. Park, R. Medishetty, J.-Y. Kim, S.S. Lee, J.J. Vittal, Angew. Chem. Int. Ed. 53 (2014) 5591-5595.

[144] Q. Chen, D.-P. Liu, J.-H. Zhu, B.-H. Han, Macromolecules 47 (2014) 5926-5931.